Acta Pharmaceutica Sinica B 2025;15(1):371−391

Chinese Pharmaceutical Association
Institute of Materia Medica, Chinese Academy of Medical Sciences

Acta Pharmaceutica Sinica B

www.elsevier.com/locate/apsb
www.sciencedirect.com

ORIGINAL ARTICLE

Drofenine as a Kv2.1 inhibitor alleviated AD-like pathology in mice through Aβ/Kv2.1/microglial NLRP3/neuronal Tau axis

Jian Lu[a,†], Qian Zhou[b,†], Danyang Zhu[c,†], Hongkuan Song[a], Guojia Xie[a], Xuejian Zhao[a], Yujie Huang[a], Peng Cao[b,d,*], Jiaying Wang[a,*], Xu Shen[a,d,*]

[a]*School of Medicine, Nanjing University of Chinese Medicine, Nanjing 210023, China*
[b]*Jiangsu Provincial Medical Innovation Center, Affiliated Hospital of Integrated Traditional Chinese and Western Medicine, Nanjing University of Chinese Medicine, Nanjing 210023, China*
[c]*School of Integrative Medicine, Nanjing University of Chinese Medicine, Nanjing 210023, China*
[d]*State Key Laboratory on Technologies for Chinese Medicine Pharmaceutical Process Control and Intelligent Manufacture, Nanjing University of Chinese Medicine, Nanjing 210023, China*

Received 28 June 2023; received in revised form 18 July 2024; accepted 18 November 2024

KEY WORDS

Alzheimer's disease;
Aβ-Tau cascade reaction;
Microglia;
NLRP3 inflammasome;
Kv2.1 channel;
Potassium efflux;
Drofenine;
Cognitive impairment

Abstract Alzheimer's disease (AD) is a neurodegenerative disease with clinical hallmarks of progressive cognitive impairment. Synergistic effects of the Aβ-Tau cascade reaction are tightly implicated in AD pathology, and microglial NLRP3 inflammasome activation drives neuronal tauopathy. However, the underlying mechanism of how Aβ mediates NLRP3 inflammasome remains unclear. Herein, we determined that oligomeric Aβ (o-Aβ) bound to microglial Kv2.1 and promoted Kv2.1-dependent potassium efflux to activate NLRP3 inflammasome resulting in neuronal tauopathy by using Kv2.1 inhibitor drofenine (Dfe) as a probe. The underlying mechanism has been intensively investigated by assays with Kv2.1 knockdown *in vitro* (*si-Kv2.1*) and *in vivo* (AAV-ePHP-*si-Kv2.1*). Dfe deprived o-Aβ of its capability to promote microglial NLRP3 inflammasome activation and neuronal Tau hyperphosphorylation by inhibiting the Kv2.1/JNK/NF-κB pathway while improving the cognitive impairment of 5×FAD-AD model mice. Our results have highly addressed that the Kv2.1 channel is required for o-Aβ-driven microglial NLRP3 inflammasome activation and neuronal tauopathy in AD model mice and highlighted that Dfe as a Kv2.1 inhibitor shows potential in the treatment of AD.

*Corresponding authors.
E-mail addresses: xshen@njucm.edu.cn (Xu Shen), wangjy@njucm.edu.cn (Jiaying Wang), cao_peng@njucm.edu.cn (Peng Cao).
[†]These authors made equal contributions to this work.

Peer review under the responsibility of Chinese Pharmaceutical Association and Institute of Materia Medica, Chinese Academy of Medical Sciences.

https://doi.org/10.1016/j.apsb.2024.11.010

1. Introduction

Alzheimer's disease (AD) is a neurodegenerative disease with clinical hallmarks of progressive cognitive impairment and memory loss and even accompanied by personality changes and mental disorders[1,2]. In late AD, the patients suffer from logical thinking loss, mobility disorder, and life-threatening complications[3]. The pathogenesis of AD is too complicated, and there is still a lack of drugs that can cure AD[4,5].

Senile plaques composed of β-amyloid (Aβ) deposition and neurofibrillary tangles formed by hyperphosphorylated Tau are two main pathological features of AD, and the occurrence and development of AD are tightly related to the synergistic effects mediated by Aβ-Tau cascade reaction[6-8]. According to the Aβ-Tau cascade reaction hypothesis, Aβ functions as a starting trigger for AD with misfolding and oligomeric forms through abnormal secretion, renders toxicities on glia and neurons inducing a series of pathological responses such as neuroinflammation and oxidative stress[7]. Furthermore, the pathological responses induced by Aβ promote the neuronal microtubule-associated protein Tau hyperphosphorylation resulting in lesions of the normal assembly function of Tau, disruption of the neuronal synaptic structure and further loss of synapse[9,10]. Notably, hyperphosphorylated Tau is self-aggregated and tends to form paired helical filaments and neurofibrillary tangles in turn causing severe neurotoxicity in neuronal cells and exacerbating Aβ pathology[11,12]. Thus, the vicious cycle between Aβ and Tau pathology highly promotes AD progression.

Microglia as the vulnerable cell population to Aβ in the central nervous system (CNS) mediates neuroinflammation in the early stage of AD pathology[13,14]. It is noted that microglial NLRP3 inflammasome activation is a key linking Aβ to Tau pathology[15], in that Aβ drives microglial NLRP3 inflammasome activation leading to the maturation and release of downstream inflammatory cytokines including IL-1β, which induces the hyperphosphorylation of Tau in neurons thereby causing further synergistic neurotoxicity and vicious cycle between Aβ and Tau pathology[7,15]. All evidence has addressed the potent role of NLRP3 inflammasome in the Aβ-Tau cascade reaction. Although many reports claimed that potassium efflux is one of the canonical pathways of NLRP3 inflammasome activation[16], the underlying mechanism of how Aβ mediates NLRP3 inflammasome activation is not clear.

Shab-related potassium channel member 1 (Kv2.1) as a voltage-gated potassium channel is composed of four α subunits (S1−S4, voltage-sensor domain; S5−S6, pore domain) and widely distributed in the CNS. The Kv2.1 channel plays an important role in regulating the outward potassium flow (about 60%) in neurons and glial cells[17]. Previous studies have shown that Kv2.1 expression level is increased in 3×Tg AD model mice[18] and the oxidative level of Kv2.1 is exacerbated in the brains of AD patients and animals[19]. All evidence has revealed the potential implication of the Kv2.1 channel in AD pathogenesis.

By considering that microglia are more vulnerable to invasion of Aβ than neurons or astrocytes[20] and that microglia-mediated neuroinflammation as one of the earliest pathological features in AD[21] mediates Aβ-Tau cascade reaction[15], we speculated that the Kv2.1 upregulation in microglia may play a more potent role than in either neurons or astrocytes in AD pathology. With these facts, we focused on the study of the regulation of Kv2.1 against microglia-mediated inflammation in our current work.

Herein, we reported that oligomeric Aβ (o-Aβ) bound to the Kv2.1 channel and promoted microglial Kv2.1-dependent potassium efflux to induce NLRP3 inflammasome activation and neuronal tauopathy by using Kv2.1 inhibitor drofenine (Dfe)[17] as a probe. The underlying mechanism has been intensively investigated by assays with Kv2.1 knockdown *in vitro* (*si-Kv2.1*) and *in vivo* (AAV-ePHP-*si-Kv2.1*). Dfe deprived o-Aβ of its capability to promote microglial NLRP3 inflammasome activation and neuronal Tau hyperphosphorylation by inhibiting the Kv2.1/JNK/NF-κB pathway while improving the cognitive impairment of 5×FAD-AD model mice. Our results have highly addressed that the Kv2.1 channel is required for o-Aβ-driven microglial NLRP3 inflammasome activation and neuronal tauopathy in AD model mice and highlighted that Dfe as a Kv2.1 inhibitor shows potential in the treatment of AD.

2. Materials and methods

2.1. Study design

The goal of the study was to evaluate the potential of Dfe in the treatment of cognitive impairment of 5×FAD-AD mice and investigate the mechanism underlying the amelioration of Dfe on AD-related pathology.

Sample sizes were chosen according to the previous experience related to AD research[22]. Investigators who conducted the experiments or analyzed the data were blinded to the group. *In vitro* assays against brain slices, primary microglia, and neurons were carried out to expound the effect of Dfe on microglial potassium current, NLRP3 inflammasome activation, neuronal tauopathy, and apoptosis. For animal studies, mice were litter and age-matched to keep all data in agreement with each other. Completely random grouping design and exploratory experimental research were performed based on the experimental animals. Novel object recognition, Y-maze, and Morris water maze tests were performed to evaluate the amelioration of Kv2.1 inhibitor Dfe on cognitive impairment of 5×FAD-AD mice. Adeno-associated virus (AAV)-ePHP-*si-Kv2.1* injection for brain-specific Kv2.1 knockdown against 5×FAD-AD mice was also performed to confirm the target of Dfe *in vivo*. Assays of histology and immunostaining of tissue sections and Western blot of brain tissues were performed to verify the conclusions of *in vitro* assays.

2.2. Materials

All cell culture reagents were purchased from Gibco. Aβ_{42} was purchased from Sigma−Aldrich. Kv2.1 inhibitor Dfe was purchased from Energy Chemical[17]. Aβ_{25-35}, JNK inhibitor SP600125 and NF-κB inhibitor pyrrolidine

dithiocarbamatemmonium (PDTC)[23] were obtained from MedChemExpress. Other reagents used in this study were purchased from Sinopharm. The purity of all compounds used in the experiments is higher than or equal to 98%. *si-Ctrl* and *si-Kv2.1* plasmids were purchased from Genepharma. AAV-ePHP-*si-NC/Kv2.1* and AAV-*cMG-f4/80-si-NC/Kv2.1* were established by WeiZhen bio, pAAV-*CX3CR1-EGFP* was purchased from OBiO Technology.

Oligomeric A$\beta_{42/25-35}$ (o-A$\beta_{42/25-35}$) was prepared according to the published approach[24]. Briefly, in preparation for Aβ oligomers, Aβ solution (10 mmol/L) was kept at a humidified incubator (5% CO_2, 37 °C) for 7 days without any agitation, and o-A$\beta_{42/25-35}$ was identified by Western blot assay (Supporting Information Fig. S1F).

2.3. GEO database bioinformatic analysis

The gene expression profile and sample information of prefrontal cortex brain tissue samples of AD patients and normal people in the GSE33000 dataset were obtained from the National Center of Biotechnology Information-Gene Expression Omnibus, which is a free database of microarray/gene profile and next-generation sequencing. In the assay, differential genes between normal people and AD patients were evaluated and compared by the criteria of LogFC. A total of 19,525 RNA-seq data points from 467 people (normal people, $n = 157$; AD patients, $n = 310$) were extracted from the dataset and 117 potassium channels were analyzed. The differential mRNA expressions of potassium ion channel-related genes of normal controls and AD cases were obtained through the acquisition of the GSE33000 dataset and data preprocessing. The expression data of related genes were visualized by GraphPad Prism 8 software.

2.4. Cell and brain slice culture

CHO-Kv2.1 cells were cultured in DMEM (Gibco) supplemented with 10% FBS (Gibco), 100 U/mL penicillin-streptomycin (Gibco), and 0.25 μg/mL puromycin (Gibco).

Primary microglia were separated from the brains of P0 mice (within 24 h of birth) according to the published approach[22]. In brief, the brain tissues were minced into small pieces and digested into a single-cell suspension with 0.25% trypsin (Gibco) and 200 U/mL DNase (Sigma−Aldrich). Then, cell fluid was *seeded* on poly-D-lysine (PDL, Sigma−Aldrich)-coated cell culture flasks at a density of 600,000 cells/mL. After 7 days, the microglia were dissociated by shaking and harvested by centrifugation at 300 × *g* (Thermo Scientific SL8R, Thermo Scientific, MA, USA) for 10 min, followed by seeding on PDL-coated cell culture plates at a density of 50,000 cells/mL. The purity of microglia was identified by immunofluorescence assay against IBa1 (Fig. S1A).

Primary neurons were separated from embryonic mouse brains (embryonic Days 16−18) according to the published approach[22]. Briefly, brain tissues were digested into a single-cell suspension with 0.125% trypsin and 200 U/mL DNase. Then, the cell fluid was *seeded* on PDL-coated cell culture flasks at 600,000 cells/mL density. After 6 h, the medium was replaced by a Neurobasal medium (Gibco) supplemented with 2% B27 (Gibco), 0.5 μmol/L L-glutamine (Sigma−Aldrich) and 50 U/μL penicillin−streptomycin. The purity of neurons was identified by immunofluorescence assay against MAP2 (Fig. S1A).

The microglial Kv2.1 specific knockdown adeno-associated virus (AAV-*cMG-f4/80-si-Kv2.1*) and the corresponding negative control AAV (AAV-*cMG-f4/80-NC*) were established and injected through lateral ventricles (1×10^{13} vg/mL, 2 μL/each side) to obtain the brain-microglial Kv2.1 knockdown mice (MG-Kv2.1-*KD*) and the negative control mice (MG-Kv2.1-*NC*). The brain slices were separated from normal or MG-Kv2.1-*NC/KD* C57/B6L mice (9 months). The assay was performed according to the published approach[25]. Mice were anesthetized with 1% pentobarbital sodium (Sigma−Aldrich) and decapitated. Mouse brain was rapidly dissected out and placed in chilled (0−3 °C) GBSS solution (1.53 mmol/L $CaCl_2$, 4.96 mmol/L KCl, 0.22 mmol/L KH_2PO_4, 0.1 mmol/L $MgCl_2$, 0.25 mmol/L $MgSO_4$, 120 mmol/L NaCl, 27 mmol/L $NaHCO_3$, 0.85 mmol/L Na_2HPO_4 and 5.5 mmol/L glucose). Brain slices (370 μm thick) were prepared by using a vibratome (VT1000 S, Leica, Wetzlar, Germany). Finally, slices were cultured with corresponding medium (50% MEM, 25% GBSS, 5% horse serum, and 20% 0.05 mol/L TBS solution) in a humidified incubator (5% CO_2, 37 °C) for 14 days.

2.5. Western blot assay

For cell samples, microglia or neurons were lysed with RIPA buffer (Beyotime) containing protease inhibitor and phosphatase inhibitor cocktails (Thermo Scientific) on ice for 20 min. For animal brain samples, brain tissues (hippocampus and cortex mixture) were homogenized with RIPA buffer supplemented with protease inhibitor and phosphatase inhibitor cocktails, and the homogenates were kept on ice for 30 min.

The supernatants of cell or tissue samples were collected by centrifuging at 12,000 × *g* (Thermo Scientific MicroCL 17R, Thermo Scientific) for 15 min at 4 °C, and protein concentration was determined by using a BCA protein assay kit (Beyotime). Protein samples were mixed with 4 × loading buffer (Thermo Scientific) and boiled for 15 min at 95 °C.

For medium samples, the mediums from brain slices or microglia were collected and centrifuged with a concentration centrifuge tube (5 kDa). Then, the concentrated medium was added to 10 times the volume of ice acetone and centrifuged at 5000 rpm (Thermo Scientific SL8R, Thermo Scientific). All proteins in the medium were re-suspended with 2 × loading buffer for subsequent Western blot assay.

All protein samples were separated by SDS-PAGE and transferred to a nitrocellulose filter membrane (GE Healthcare) by using a Gel electrophoresis system (Mini-PROTEAN Tetra, Bio-Rad, CA, USA). After blocking at room temperature for 2 h, the membranes were incubated with the corresponding antibodies (1:1000; Supporting Information Table S1) overnight at 4 °C. Then, the membranes were washed three times and incubated with secondary antibodies (1:3000) conjugated with horseradish peroxidase (Jackson) at room temperature for 2 h. The blots were developed and visualized by using the Gel imaging system (Tanon 5200, Tanon, Shanghai, China).

Cropped blots were performed to detect the levels of proteins with different molecular weights.

2.6. Immunofluorescence staining assay

For immunofluorescence staining assay against cell samples, primary microglia or neurons were washed three times with PBS and fixed in 4% paraformaldehyde (Solarbio) at room temperature for 30 min. Cells were incubated with PBST (5% Triton X-100, Beyotime) for 15 min and blocked by 5% BSA (Solarbio) at room temperature for 1 h, followed by incubation with the primary

antibodies (1:300) overnight at 4 °C. Then, the cells were washed three times with PBS and incubated with corresponding fluorescent secondary antibodies (anti-goat, anti-rabbit, or anti-mouse; dilution 1:500) at 37 °C for 1 h in the dark. The nuclear was stained by using Hoechst 33342. The images were acquired by using a microscope (DMi8, Leica, Wetzlar, Germany).

For immunohistochemistry assay against brain tissues, the brain slides were incubated with PBST for 15 min and blocked in 5% BSA at room temperature for 1 h, followed by incubation with the primary antibody (1:300; Supporting Information Table S2) overnight at 4 °C. The slides were washed with PBS and incubated with fluorescent secondary antibodies (1:500) for 2 h. The slides were imaged using a microscope (DMI8, Leica, Wetzlar, Germany) and the images were analyzed by the Image J software.

2.7. *siRNA plasmid transfection*

For *siRNA* plasmid transfection, primary microglia or neurons were seeded at a density of 50,000 cells/mL on PDL-coated 24-cell culture plates. After 24 h, the cells were transfected with *si-Ctrl* or *si-Kv2.1* plasmid using Lipofectamin 2000 transfection reagent (Invitrogen). After 48 h, Kv2.1 knockdown efficiency by *siRNA* was detected by Western blot assay. As indicated in Fig. S1B−S1E, the Kv2.1 protein level was reduced by about 80% after *siRNA* transfection in primary microglia or neurons.

2.8. *Intracellular potassium level assay*

Intracellular potassium level measurement was performed by using the MX4521-Enhanced Potassium Green-4 AM indicator (EPG-4, MaoKangbio) according to the manufacturer's protocol. Microglia or neurons were loaded with EPG-4 probes (1 μmol/L) for 2 h and cultured with serum-free medium for 1 h. Intracellular potassium level was detected by using a fluorescence microscope (DMI8, Leica, Wetzlar, Germany).

2.9. *Electrophysiological recording assay*

The whole-cell patch clamp recordings against CHO-Kv2.1 cells or brain slices were performed according to the published approach[17].

CHO-Kv2.1 cells were seeded at a density of 1000 cells/mL on 12 cell culture plates. The cells were pre-treated with Dfe (10 μmol/L) for 0.5 h and co-treated with o-Aβ_{25-35} (5 μmol/L) for 12 h. In the assay against CHO-Kv2.1 cells, pipettes were filled with a solution containing 140 mmol/L KCl, 2 mmol/L $MgCl_2$, 10 mmol/L EGTA, 1 mmol/L $CaCl_2$, and 10 mmol/L HEPES (pH 7.3), and cells were bath-perfused with a solution containing 150 mmol/L NaCl, 5 mmol/L KCl, 0.5 mmol/L $CaCl_2$, 1.2 mmol/L $MgCl_2$ and 10 mmol/L HEPES (pH 7.3).

In the assay against brain slices, microglia in the brain of mice were labeled by lateral ventricle injection with pAAV-*CX3CR1-EGFP* (Fig. S1H, 1×10^{13} vg/mL, 2 μL/each side), and microglial-specific Kv2.1 knockdown by AAV-*cMG-f4/80-si-Kv2.1* injection were also constructed. The infection efficiency was detected two weeks after AAV injection, and a large number of microglia with green fluorescence in the brains of mice were determined (Fig. S1H). Mice were anesthetized with 1% pentobarbital sodium and decapitated. Mouse brain was rapidly dissected out and placed in chilled (0−3 °C) potassium current-artificial cerebrospinal fluid (K^+-ACSF, 130 mmol/L NaCl, 5.4 mmol/L KCl, 1 mmol/L $MgCl_2$, 10 mmol/L HEPES, 2 mmol/L $CaCl_2$, 1 μmol/L TTX, 0.3 mmol/L $CdCl_2$ and 10 mmol/L glucose, pH 7.3). Brain slices (370 μm thick) were prepared by using a vibratome (VT1000 S, Leica, Wetzlar, Germany) and incubated in continuously oxygenated (95% O_2, 5% CO_2) K^+-ACSF at 37 °C for 0.5 h. A slice was then transferred to a submersion-type recording chamber (Molecular Devices, CA, USA) and immersed in K^+-ACSF continuously oxygenated. Pipettes were filled with a solution containing 120 mmol/L KCl, 1 mmol/L $MgCl_2$, 10 mmol/L EGTA, 1 mmol/L $CaCl_2$, and 5 mmol/L HEPES (pH 7.3).

The current signals were filtered at 1 kHz and digitized at a 10 kHz sampling frequency by using DigiData 1440 A (Molecular Devices) and analyzed with pClamp 10.2 software (Molecular Devices). Whole-cell Kv2.1 potassium currents were recorded using the protocol: the holding potential was set at −80 mV and stepwise depolarized from −80 to +60 mV in 10 mV (for brain slices, from −80 to +80 mV in 20 mV) increments and then repolarized to −80 mV. The effect of o-Aβ_{25-35} or Dfe on Kv2.1 channel activation was recorded using the protocol as follows: the holding potential was set at −80 mV and stepwise depolarized from −80 to +60 mV in 10 mV increments and then repolarized to −40 mV. The effect of o-Aβ_{25-35} or Dfe on Kv2.1 channel inactivation was recorded using the protocol as follows: the holding potential was set at −80 mV and stepwise depolarized from −80 to +60 mV in 10 mV increments.

2.10. *Kv2.1 channel-related assay*

Kv2.1 channel-related assay was performed according to our previously published approach by using a membrane potential assay kit (Molecular Devices)[23]. CHO-Kv2.1 cells were seeded at a density of 50,000 cells/mL on 48 cell culture plates. Briefly, CHO-Kv2.1 cells were co-incubated with cellular membrane potential detection solution (voltage-sensitive fluorescent indicators and membrane dyes) for 0.5 h. Then, the membrane potential assay was conducted by using a Flex station III instrument (Molecular Devices).

2.11. *Flow cytometry*

The flow cytometry assay against single cells isolated from animal brain tissues was performed to detect the protein levels of Kv2.1 in different cell populations. In the assay, neurons, microglia, and astrocytes were respectively labeled by MAP2, IBa1, and GFAP flow antibody (Proteintech; CL647-66827, CL594-17490, CL488-60190). The single-cell suspensions of the hippocampus and cortex were prepared by using GentleMACSTM Octo according to the manufacturer's protocol (Miltenyi Biotec).

The neuronal apoptosis was detected by using the Annexin V-FITC/PI apoptosis detection kit (KeyGen) according to the manufacturer's protocol. A flow cytometer (Intellicyt® iQue3, Sartorius, Gottingen, Germany) was used to detect the proportion of cell apoptosis.

2.12. *Animals*

All animal experiments comply with the ARRIVE guidelines and were carried out in accordance with the U.K. Animals (Scientific Procedures) Act, 1986. All animals were maintained under standard conditions at room temperature (22 °C) by a 12 h light/dark cycle. The animal experiments were approved by the

Experimental Animal Ethics Committee of Nanjing University of Chinese Medicine (No. 202008A002).

Female wild-type (WT) and 5×FAD transgenic (APPSwFlLon, PSEN1×M146L×L286V) mice were obtained from a breeding pair purchased from the Jackson Laboratory agency by Nanjing Institute of Biomedicine (Nanjing, China). The 5×FAD-AD mice overexpress human amyloid precursor protein (APP) and human presenilin 1 (PS1) with five mutations associated with familial Alzheimer's disease: mutations of Swedish (K670N, M671L) Florida (1716V) and London (V717I) in APP and PS1 (M146L and L286V) were identified by gel electrophoresis assay against mutated APP and PS1 genes (Fig. S1G). Brain-specific Kv2.1 knockdown 5×FAD-AD mice were established by injecting AAV-ePHP-*si-Kv2.1* (AAV-*si-Kv2.1*, 5×10^{11} vg/mouse) through tail vein against the mice at the age of six and a half months. AAV-*si-NC* (NC, virus negative control) was injected into WT or 5×FAD-AD mice at the age of six and a half months to establish negative or positive control group in the assay. Kv2.1 knockdown efficiency of AAV-*si-Kv2.1* in 5×FAD-AD mice were evaluated and the results indicated that AAV-*si-Kv2.1* injection effectively reduced the protein level of Kv2.1 channel in either brain (Supporting Information Fig. S6A−S6C) or microglia (Fig. S6D and S6E) of female and male 5×FAD-AD mice at the age of 9 months, respectively.

Experimental mice were divided into WT mice treated with the vehicle group (female, $n = 10$ per group), WT mice treated with Dfe-10 mg/kg/day group (WT + Dfe; female, $n = 10$ per group), 5×FAD-AD mice treated with the vehicle group (5×FAD; female, $n = 10$ per group), 5×FAD-AD mice treated with Dfe-10 mg/kg/day group (5×FAD + Dfe; female, $n = 10$ per group), WT mice injected with AAV-*si-NC* and treated with the vehicle group (WT-*NC*; female, $n = 10$ per group), 5×FAD-AD mice injected with AAV-*si-NC* and treated with the vehicle group (5×FAD-*NC*; female, $n = 10$ per group), 5×FAD-AD mice injected with AAV-*si-Kv2.1* and treated with vehicle group (5×FAD-*KD*; female, $n = 10$ per group) and 5×FAD-AD mice injected with AAV-*si-Kv2.1* and treated with Dfe-10 mg/kg/day group (5×FAD-*KD* + Dfe; female, $n = 10$ per group). Dfe was dissolved in normal saline, and administration of Dfe in mice at 10 mg/kg/day was referenced by our previous work[17]. Experimental mice were treated with vehicle or Dfe by intraperitoneal injection for 8 weeks.

2.13. Behavioral test

2.13.1. Novel object recognition (NOR) test

The test was performed according to the published approach[22]. Briefly, the test consisted of four sequential daily trials. In the *adaptation* trial on Days 1 and 2, mice were placed in the center of the apparatus and allowed to freely explore the space in the absence of any objects for 15 min. In the acquisition trial on Day 3, mice were placed in the apparatus again in the presence of two identical objects and allowed to freely explore the space for 10 min. Finally, the memory test was performed on Day 4. One of the familiar objects was replaced by a novel object with differences in its shape, color, and texture. The mice were allowed to freely explore both objects for 10 min. All trial data were collected for animal performance analysis. The discrimination index (DI) is calculated as the difference between the time spent exploring the novel (TN) and the familiar object (TF) divided by the total exploration time (TN+TF), as shown in Eq. (1):

$$DI = [TN\text{-}TF]/[TN+TF] \quad (1)$$

2.13.2. Y-maze test

The test was performed according to the published approach[22]. Briefly, during the learning trial, an arm (novel arm) was blocked by an opaque door. The mice were allowed to freely explore the other two arms (familiar arms) for 5 min and returned to their home cages. Two hours later, the mice were returned to the maze and allowed to explore all three arms for 5 min. All trial data were collected for animal performance analysis.

2.13.3. Morris water maze (MWM) test

The test was performed according to the published approach[22]. During training trials, the invisible submerged platform was placed in the circular pool filled with milk. Then, the mice were given 60 s to search for the platform and allowed to stay at the platform for 10 s. If the mice failed to find the platform within 60 s, the mice were gently placed onto the platform and kept there for 10 s. The training trials were continuously performed three times a day for 7 days. The probe trial was carried out on the eighth day. Then, the platform was removed, and the mice were allowed to search for the platform for 60 s. All trial data were collected for animal performance analysis.

2.14. Hepatotoxicity and nephrotoxicity assays

The levels of ALT, AST, Urea, and CR in serum were detected by using commercialized reagent kits (Kings Bio) following the manufacturer' s instructions.

2.15. AT8 staining assay

AT8 staining assay was performed to detect the levels of p-Tau at sites of Ser202 and Thr205 in the hippocampus of 5×FAD-AD mice. Briefly, the brain slides were incubated with PBST for 15 min and blocked in 5% BSA at room temperature for 1 h, followed by incubation with AT8 antibody (1:300) overnight at 4 °C. Then, the slides were incubated with secondary antibodies-HRP (1:500) for 2 h and visualized by using a DAB solution (Beyotime). Finally, the slides were imaged using a microscope (DM1000, Leica, Wetzlar, Germany) and the images were analyzed by the ImageJ software.

2.16. Long-term potentiation (LTP) assay

Mice were anesthetized with 1% pentobarbital sodium and decapitated. Mouse brain was rapidly dissected out and placed in chilled (0−3 °C) artificial cerebrospinal fluid (ACSF, 126 mmol/L NaCl, 2.5 mmol/L KCl, 1.25 mmol/L NaH_2PO_4, 2 mmol/L $MgSO_4$, 2 mmol/L $CaCl_2$, 26 mmol/L $NaHCO_3$ and 10 mmol/L glucose). Brain slices (370 μm thick) were prepared by using a vibratome (VT1000 S, Leica, Wetzlar, Germany) and incubated in continuously oxygenated (95% O_2, 5% CO_2) ACSF at 37 °C for 0.5 h. A slice was then transferred to a submersion-type recording chamber (Molecular Devices) and immersed in ACSF continuously oxygenated.

In the LTP assay, the field potential signal in the resting state was recorded for 10 min as the baseline. LTP in the hippocampal DG region was stimulated by 4 × 100-Hz stimuli and the field potential signal after stimulating was recorded for 60 min. The

strength of synaptic transmission was determined by measuring the initial slope (20%−80% rising phase) of field excitatory postsynaptic potentials. Six brain slices from three animals for each group were recorded and used to calculate the means.

2.17. TUNEL staining assay

TUNEL staining assay was performed to detect neuronal apoptosis in the hippocampus of 5×FAD-AD mice by using the One Step *TUNEL* Apoptosis Assay Kit (Beyotime) according to the manufacturer's protocol[22]. The slides were imaged using a fluorescence microscope (DMI8, Leica, Wetzlar, Germany) and the images were analyzed by the Image J software.

2.18. Nissl staining assay

Nissl staining assay was performed to detect neuronal nuclear in the hippocampus of 5×FAD-AD mice using the Nissl Staining Solution-Cresyl Violet (Solarbio) according to the manufacturer's protocol[26]. The slides were imaged using a microscope (DMI8, Leica, Wetzlar, Germany) and the images were analyzed by the Image J software.

2.19. Statistical analysis

All data were presented as mean ± standard error of mean (SEM), and statistical $P < 0.05$ was significant. The *t*-test was performed to analyze the significant difference between two groups. For the animal assay, two-way ANOVA with Fisher's LSD test was performed to analyze the significant differences among multiple treatment groups. For cell assay, one-way ANOVA with Dunnett's post-test was performed to analyze the significant difference among multiple treatment groups. The data were analyzed for statistical significance using the graphing program GraphPad Prism 8. The significance analysis of all experimental results was marked in the Figures.

3. Results

3.1. Microglial Kv2.1 channel was upregulated in AD pathology

3.1.1. mRNA level of Kv2.1 was upregulated in AD patients

Given the pivotal role of potassium efflux in AD-related pathologies including inflammatory response and neuronal apoptosis, a public GEO database (GSE33000[27]) was analyzed to identify the potassium channels with differential expressions in brains of normal and AD individuals. In the analysis, typical types of potassium channels were selected including potassium voltage-gated channels, potassium inwardly-rectifying channels, and calcium-dependent potassium channels (LogFC). A total of 117 potassium channels within the GSE33000 database (normal people, $n = 157$; AD patients, $n = 310$) were analyzed, and the results (Fig. 1A and B) indicate that the mRNA levels of *KCNB1* (Kv2.1) and *KCNG1* (Kv6.1) potassium channels were increased in AD patients. By considering that Kv6.1 cannot form a functional channel alone and only forms a functional hetero-tetrameric channel through binding with the Kv2.1 channel[28], we speculated that the Kv2.1 channel might be the key potassium mediator in AD development.

3.1.2. Kv2.1 protein level was upregulated in APP/PS1 and 5×FAD-AD mice

With above-mentioned facts, Kv2.1 expressions in brains of two types of AD model mice (APP/PS1 and 5×FAD-AD mice constructed by Aβ pathology[29,30]) were thus detected by Western blot assay, and the results indicate that the protein levels of cerebral Kv2.1 channel in APP/PS1 or 5×FAD-AD mice were increased compared with those in WT mice (Fig. 1C and D).

Furthermore, considering the different responses mediated by Kv2.1 in different cells, investigation of Kv2.1 expression in neurons, microglia, or astrocytes in WT and 5×FAD-AD mice was performed by immunofluorescence assay. Neurons, microglia, and astrocytes were labeled by MAP2, IBa1, and GFAP, respectively. As shown in Fig. 1E and F, among the above three cell populations, the Kv2.1 channel was predominantly expressed in neurons and microglia. Notably, Kv2.1 expression was elevated in microglia but slightly upregulated in neurons of 5×FAD-AD mice compared with that in WT mice. Moreover, the results of flow cytometry against single cell isolated from animal brain tissue (neurons, microglia, and astrocytes were respectively labeled by MAP2, IBa1, and GFAP flow antibody) were in line with the immunofluorescence assay results (Fig. 1G).

All results thus suggest that microglial Kv2.1 dysfunction was mainly involved in AD progression.

3.1.3. o-Aβ bound to Kv2.1 channel

Next, to further identify the interaction between Aβ and Kv2.1 channel in different cells, co-localization of Aβ and Kv2.1 in neurons, microglia, or astrocytes in brain of 5×FAD-AD mice were detected by immunofluorescence assay. As shown in Fig. 1H and I, there was a large number of co-localization areas of Aβ with microglial Kv2.1 and rare co-localization areas of Aβ with neuronal or astrocytic Kv2.1. These results thereby suggest that Aβ mainly regulated the microglial Kv2.1 channel in the brain of 5×FAD-AD mice.

Additionally, a Co-IP assay against brain tissues of APP/PS1 and 5×FAD-AD mice and a cellular thermal shift assay (CETSA) against CHO-Kv2.1 cells were also performed to confirm the direct binding of Aβ to Kv2.1 channel *in vivo* and *in vitro*. As shown in Fig. 1J, Co-IP assay results indicate that there was a direct combination between o-Aβ (∼40 kDa, Aβ decamer/dodecamer[31,32]) and Kv2.1 channel in brains of both APP/PS1 and 5×FAD-AD mice, while there was no such combination between o-Aβ and Kv2.1 channel in WT mice due to the low expression of Aβ. Moreover, the CETSA result (Fig. 1K and L) indicates that the Kv2.1 channel in o-A$\beta_{42/25-35}$-treated cell lysate showed better stability than the DMSO-treated group, and o-A$\beta_{42/25-35}$ rendered no influence on the denaturing temperatures of control protein GAPDH. These results thus demonstrated that Aβ bound with Kv2.1 channel and stabilized the membrane Kv2.1 channel. Notably, no difference was determined in the binding ability with the Kv2.1 channel between o-Aβ_{25-35} and o-Aβ_{42}.

Thus, all results implied that Aβ mediated AD pathology involving binding with microglial Kv2.1 channel, and we focused on the investigation of Aβ/microglia/Kv2.1/NLRP3 inflammasome axis in our follow-up study.

3.2. Dfe suppressed o-Aβ mediated microglial potassium efflux by inhibiting the Kv2.1 channel

By considering that the Kv2.1 channel is a major channel in regulating cellular potassium outflow, we investigated whether Aβ

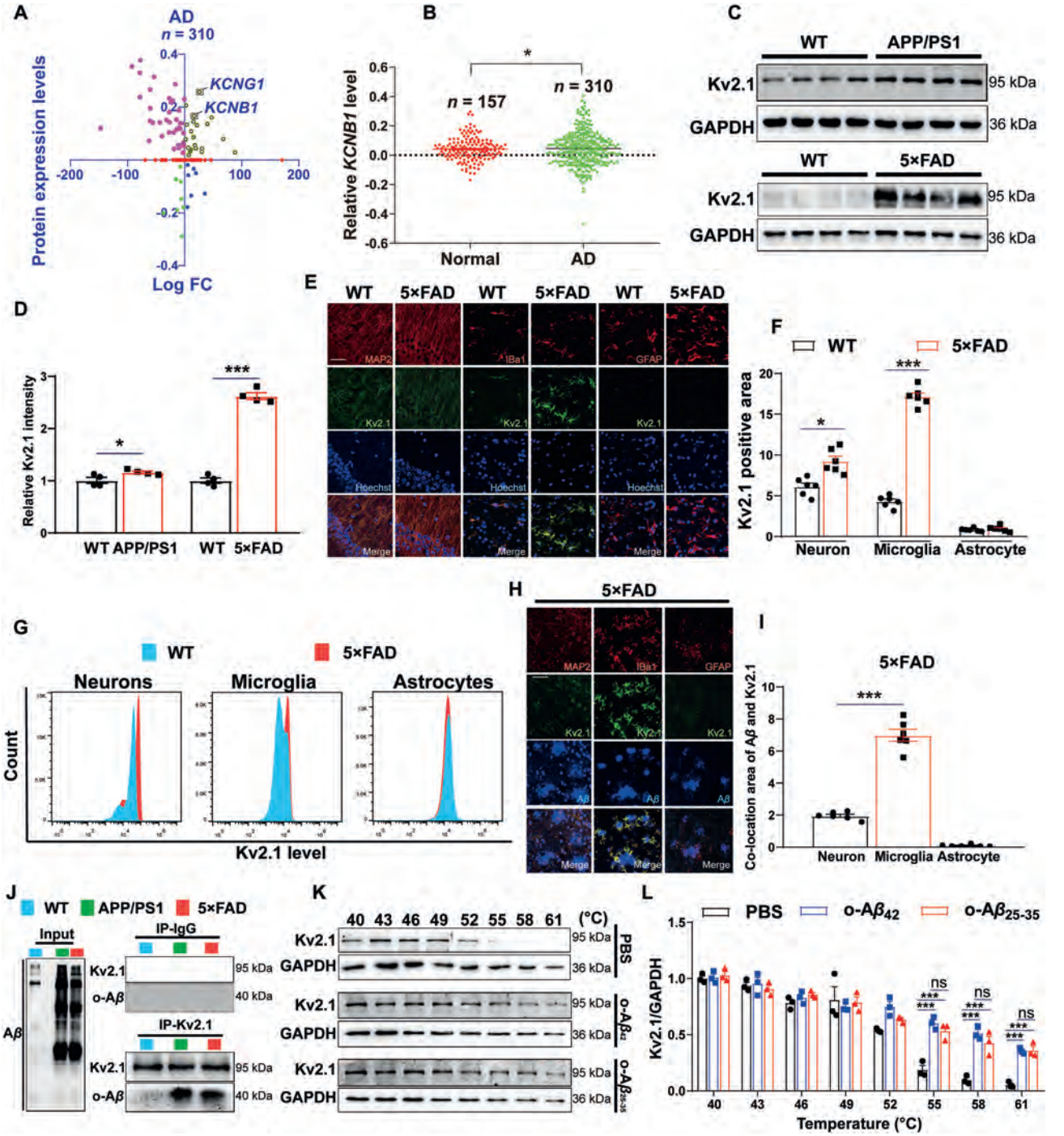

Figure 1 Microglial Kv2.1 channel was upregulated in AD pathology. (A) GEO data assay results indicated that Kv2.1 and Kv6.1 channels were highly expressed in the brains of AD patients ($n = 310$). (B) GEO data assay results indicate that the mRNA level of the Kv2.1 channel in the brains of AD patients was higher than that of normal individuals (Normal, $n = 157$; AD, $n = 310$). (C) Western blot assay and (D) its quantification results indicate that the protein level of Kv2.1 in the brains of APP/PS1 or 5×FAD-AD mice was higher than that of WT mice ($n = 4$). (E) Immunofluorescence assay and (F) its quantification results demonstrate that the microglial Kv2.1 channel was regulated in the brain of 5×FAD-AD mice. Scale bar: 80 μm ($n = 6$). (G) The flow cytometry against single cells isolated from animal brain tissue result indicated that Kv2.1 expression was obviously elevated in microglia and slightly upregulated in neurons, while unchanged in astrocytes of 5×FAD-AD mice compared with that in WT mice ($n = 3$). (H) Immunofluorescence assay and (I) its quantification results demonstrated that Aβ mainly co-localized with microglial Kv2.1 channel in the brain of 5×FAD-AD mice. Scale bar: 80 μm ($n = 6$). (J) Co-IP results indicated that Aβ directly bound to the Kv2.1 channel in the brains of APP/PS1 or 5×FAD-AD mice ($n = 3$). (K) CETSA assay and (L) its quantification results indicated that either o-Aβ_{42} or o-Aβ_{25-35} directly bound to the Kv2.1 channel in CHO-Kv2.1 cell ($n = 3$). All values are presented as mean ± SEM. ns, not significant; $^*P < 0.05$, $^{**}P < 0.01$, $^{***}P < 0.001$ compared by *t*-test.

promoted microglial potassium efflux through the Kv2.1 channel by using a published Kv2.1 inhibitor Dfe[17]. Accordingly, due to the similar capabilities of o-Aβ_{25-35} and o-Aβ_{42} in binding with the Kv2.1 channel (Fig. 1J and K), o-Aβ_{25-35} (abbreviated as o-Aβ, if not specified hereafter) was used to activate NLRP3 inflammasome (Supporting Information Fig. S2A−S2E) and regulate potassium level (Fig. S2F and S2G) in the following assays.

3.2.1. Dfe suppressed o-Aβ mediated Kv2.1-dependent potassium outward current

A patch clamp electrophysiology assay against CHO-Kv2.1 cells was carried out to inspect whether o-Aβ enhanced Kv2.1-dependent potassium outward current. In the assay, CHO-Kv2.1 cells[17] were pre-treated with or without Dfe (10 μmol/L) for 0.5 h and then co-treated with o-Aβ (5 μmol/L) for 12 h. As shown in Fig. 2A−D, o-Aβ upregulated outward potassium current and density, while Dfe deprived o-Aβ of its above capability in CHO-Kv2.1 cells. Moreover, results of membrane potential assay against CHO-Kv2.1 cells also indicated that o-Aβ enhanced Kv2.1-dependent membrane potential (Fig. 2E). Thus, all results demonstrated that o-Aβ enhanced potassium efflux through the Kv2.1 channel.

Additionally, to inspect the mechanism underlying the o-Aβ-induced potassium efflux from the perspective of kinetics, Kv2.1 channel activation/inactivation assays were also performed through a whole cell patch clamp. As shown in Supporting Information Fig. S3A−S3H, neither o-Aβ nor Dfe affected the activation state of the Kv2.1 channel (Fig. S3A−S3D), but both o-Aβ and Dfe delayed the inactivation state of the Kv2.1 channel (Fig. S3E−S3H). Interestingly, pre-treatment of Dfe abolished such an effect of o-Aβ on the Kv2.1 channel inactivation state (Fig. S3E−S3H). These results thus suggested that Dfe might suppress o-Aβ-induced potassium leakage through non-competitive binding to the Kv2.1 channel[17].

3.2.2. Dfe suppressed o-Aβ-mediated microglial potassium efflux in brain slices

To further confirm that Aβ mediated microglial potassium efflux through the Kv2.1 channel, a patch clamp electrophysiology assay against brain slice was carried out. In the assay, microglia in the brain of mice were labeled by lateral ventricle injection with pAAV-*CX3CR1-EGFP* (Fig. S1H, 1×10^{13} vg/mL, 2 μL/each side), and microglial specific Kv2.1 knockdown by AAV-*cMG-f4/80-si-Kv2.1* injection were also constructed. The infection efficiency was detected two weeks after AAV injection, and a large number of microglia with green fluorescence in the brains of mice were determined (Fig. S1H). As shown in Fig. 2F−H, o-Aβ (20 μmol/L) effectively strengthened potassium efflux in microglia of brain slice, and Dfe (10 μmol/L) suppressed o-Aβ induced microglial potassium efflux. Additionally, Kv2.1 channel knockdown by microglial-specific Kv2.1 knockdown also deprived Aβ of its ability to induce microglial potassium efflux and Dfe failed to regulate microglial potassium current in brain slices with Kv2.1 knockdown (Fig. 2F−H). All these results indicated that Aβ mediated microglial potassium efflux through the Kv2.1 channel and Dfe suppressed o-Aβ-induced microglial potassium efflux by inhibiting the Kv2.1 channel.

3.2.3. Dfe suppressed o-Aβ-induced microglial potassium efflux by inhibiting the Kv2.1 channel

Finally, a potassium probe EPG-4 was also used to investigate whether o-Aβ induced microglial potassium efflux through the Kv2.1 channel. As shown in Fig. 2I and J, o-Aβ decreased intracellular potassium levels in microglia, and Kv2.1 inhibitor Dfe (10 μmol/L) antagonized the o-Aβ-induced decline in intracellular potassium level. Notably, *si-Kv2.1* treatment deprived either o-Aβ of its capability in suppressing intracellular potassium level or Dfe of its capability in antagonizing the o-Aβ-induced decline in intracellular potassium level. These results demonstrated that Dfe suppressed o-Aβ-induced microglial potassium efflux by inhibiting the Kv2.1 channel.

Thus, all results demonstrate that o-Aβ promoted microglial potassium efflux through the Kv2.1 channel and Dfe suppressed o-Aβ-mediated microglial potassium efflux by inhibiting the Kv2.1 channel.

3.3. Dfe inhibited o-Aβ-mediated microglial NLRP3 inflammasome activation through Kv2.1/JNK/NF-κB pathway

Considering the role of the Kv2.1 channel in the regulation of extracellular potassium and the critical role of potassium efflux in microglial NLRP3 inflammasome activation, we detected the effect of Dfe on o-Aβ-mediated NLRP3 inflammasome activation.

3.3.1. Dfe suppressed o-Aβ-induced NLRP3 inflammasome activation through microglial Kv2.1 in brain slices

Cultured brain slices were used to simulate the cellular environment in the brain and o-Aβ treatment (20 μmol/L) was used to mimic the pathological condition of AD *in vitro*. Immunofluorescence and Western blot assays against brain slices were performed to evaluate the inhibitive effect of Dfe on o-Aβ-induced NLRP3 inflammasome activation and the results (Fig. 3A−D) indicated that o-Aβ increased NLRP3-ASC positive areas in brain slices and the level of inflammatory cytokines IL-1β in culture medium, while Dfe (5 and 10 μmol/L) treatment reduced the NLRP3-ASC positive areas and the level of IL-1β in culture medium from o-Aβ-treated brain slices. These results thus indicate that Dfe suppressed the o-Aβ-induced NLRP3 inflammasome activation in brain slices.

To investigate the critical role of microglial Kv2.1 in o-Aβ-induced NLRP3 inflammasome activation, a microglial Kv2.1 specific knockdown adeno-associated virus (AAV-*cMG-f4/80-si-Kv2.1*) and corresponding negative control AAV (AAV-*cMG-f4/80-NC*) were established and injected through lateral ventricles to obtain the brain-microglial Kv2.1 knockdown mice (MG-Kv2.1-*KD*) and the negative control mice (MG-Kv2.1-*NC*). The knockdown efficiency of AAV-*cMG-f4/80-si-Kv2.1* against microglial Kv2.1 was shown in Supporting Information Fig. S4A and S4B.

Then, the brain slices from MG-Kv2.1-*NC* and MG-Kv2.1-*KD* mice were prepared, followed by treatment with DMSO, o-Aβ, and o-Aβ+Dfe, respectively. Notably, AAV-*cMG-f4/80-si-Kv2.1* injection (*i.e.*, brain-microglial Kv2.1 specific knockdown) effectively reduced the NLRP3-ASC positive areas in brain slices, while Dfe had no impacts on NLRP3 inflammasome in MG-Kv2.1-*KD* brain slices (Fig. 3E−G). All results thus indicated that microglial Kv2.1 was responsible for o-Aβ-induced NLRP3 inflammasome activation and Dfe suppressed such NLRP3 inflammasome activation through microglial Kv2.1.

3.3.2. Dfe suppressed o-Aβ induced NLRP3 inflammasome activation in microglia by inhibiting the Kv2.1 channel

Additionally, cultured primary microglia were also applied in the following assays to further confirm the antagonism effect of Dfe

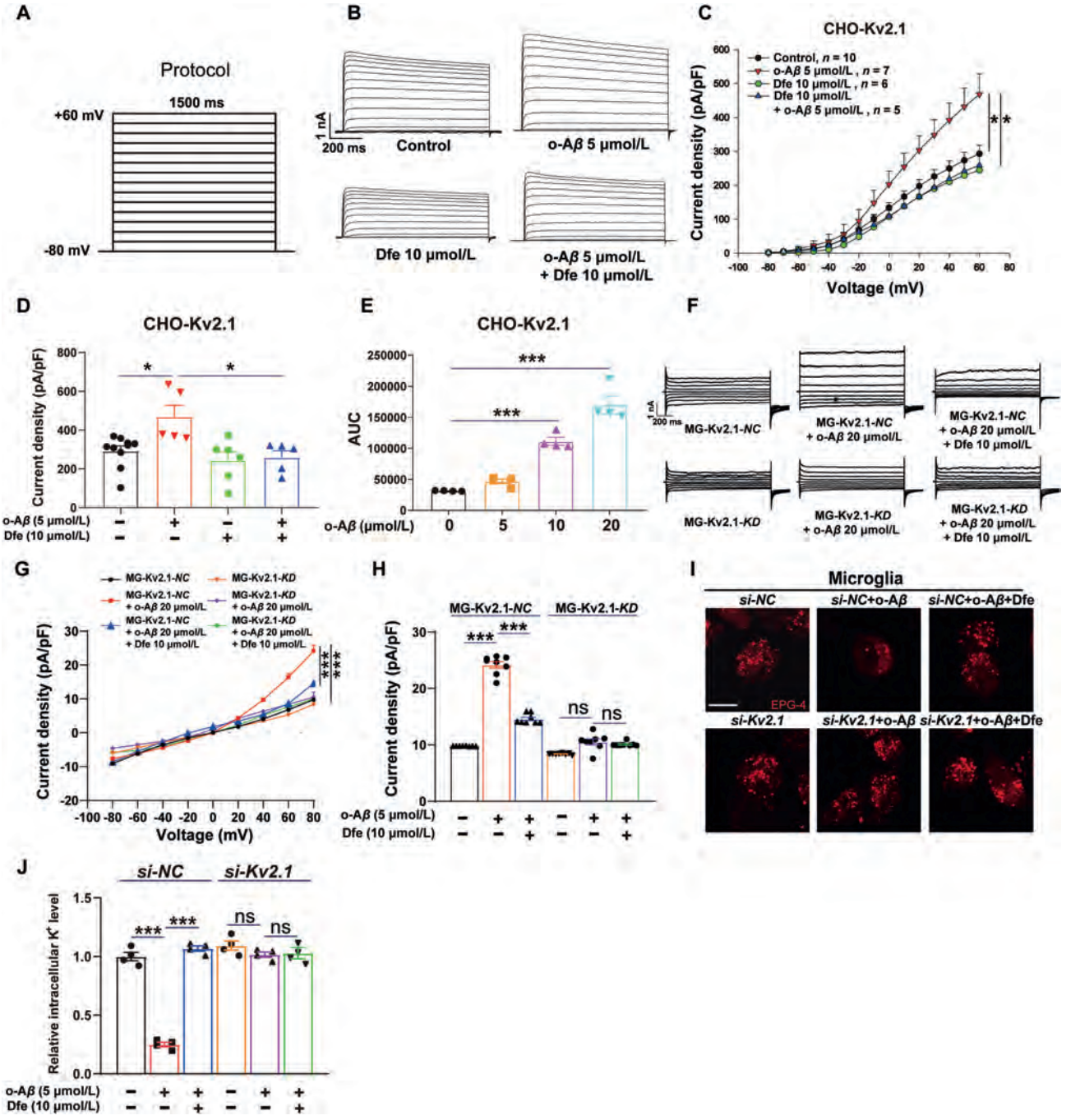

Figure 2 Dfe suppressed o-Aβ mediated microglial potassium efflux by inhibiting the Kv2.1 channel. (A) The protocol of whole cell patch clamp assay against CHO-Kv2.1 cells and brain slices. (B) Whole-cell patch clamp assay against CHO-Kv2.1 cells and (C, D) its quantification results indicated that o-Aβ upregulated outward potassium current and its density, and treatment of Kv2.1 inhibitor Dfe deprived o-Aβ of such a capability in CHO-Kv2.1 cells (n = 5−10). (E) Membrane potential assay results showed that o-Aβ upregulated Kv2.1-dependent membrane potential in CHO-Kv2.1 cells (n = 4). (F) Whole-cell patch clamp assay against brain slices and (G, H) its quantification results indicated that o-Aβ upregulated microglial outward potassium current and its density, and treatment of Kv2.1 inhibitor Dfe deprived o-Aβ of such a capability in brain slices (n = 8). (I) EPG-4 potassium probe-based assay and (J) its quantification results demonstrated that Dfe treatment antagonized the o-Aβ-induced reduction of microglial intracellular potassium level, and Dfe failed to regulate potassium level in *si-Kv2.1*-treated microglia. Scale bar: 50 μm (n = 4). All values are presented as mean ± SEM. ns, not significant; *$P < 0.05$, ***$P < 0.001$ compared by one-way ANOVA test.

on o-Aβ-mediated NLRP3 inflammasome activation. As shown in Fig. 3H and I, o-Aβ upregulated the protein expressions of NLRP3, p-NLRP3, ASC, Cas1 (p20) and IL-1β, while Dfe treatment antagonized the o-Aβ-induced upregulation of these proteins, which is in line with the immunofluorescence results that Dfe treatment reduced the number of NLRP3-ASC positive puncta in microglia (Fig. 3J and K). Notably, o-Aβ lost its capability in activating NLRP3 inflammasome and Dfe failed to regulate

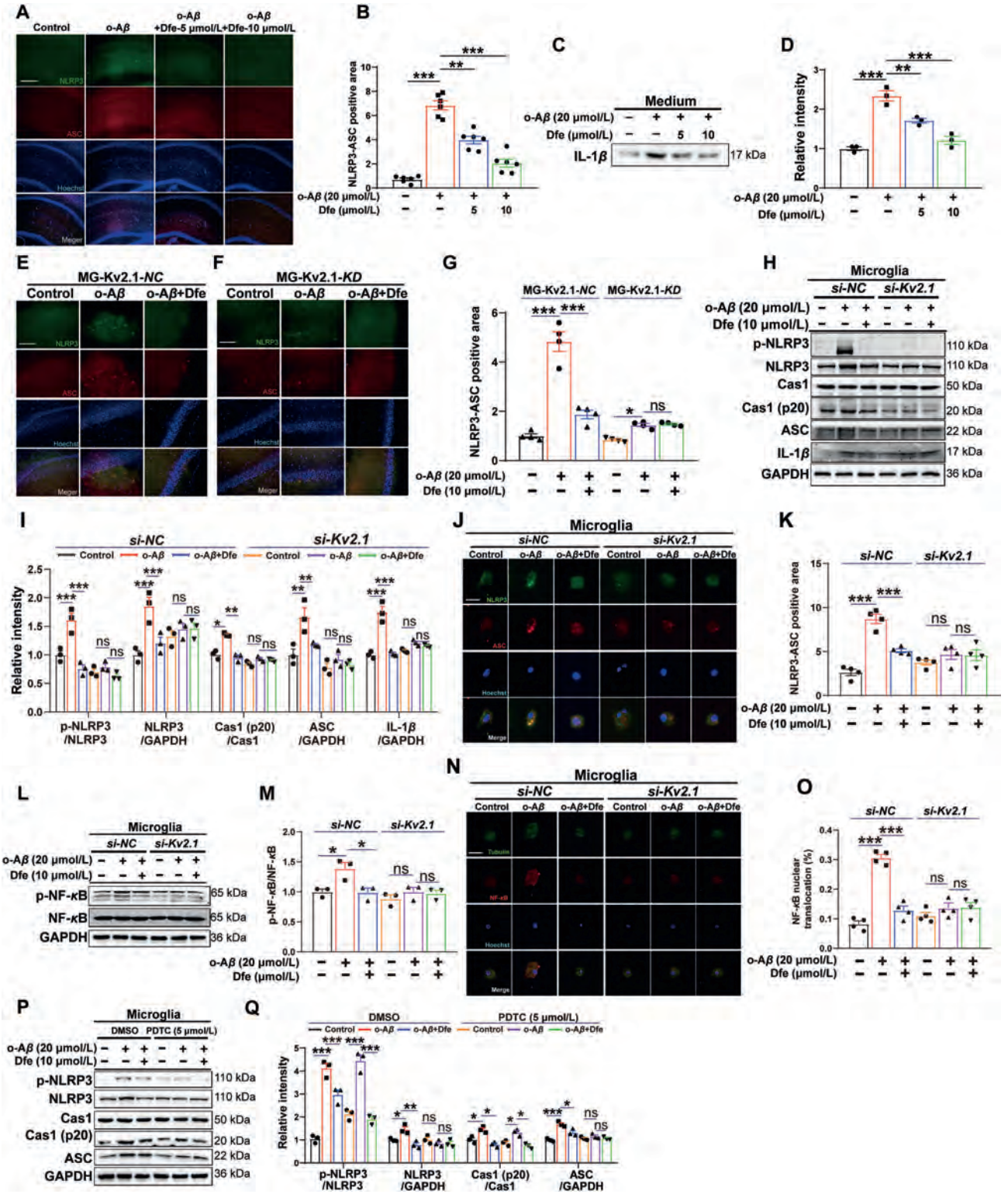

Figure 3 Dfe inhibited o-Aβ-mediated microglial NLRP3 inflammasome activation through Kv2.1/JNK/NF-κB pathway in microglia. (A) Immunofluorescence assay and (B) its quantification results demonstrated that Dfe treatment suppressed o-Aβ-mediated NLRP3 inflammation activation in brain slices. Scale bar: 200 μm (n = 6). (C) Western blot assay and (D) its quantification results indicated that Dfe treatment reduced the level of IL-1β in the medium form o-Aβ-treated brain slices (n = 3). (E, F) Immunofluorescence assay and (G) its quantification results demonstrated that Dfe treatment reduced the NLRP3-ASC positive areas in brain slices and Dfe had no impacts on NLRP3 inflammasome in MG-Kv2.1-*KD* brain slices. Scale bar: 100 μm (n = 4). (H) Western blot assay and (I) its quantification results indicated that Dfe treatment antagonized o-Aβ-induced upregulation of NLRP3, p-NLRP3, ASC, Cas1 (p20), and IL-1β in microglia, and Dfe failed to regulate these NLRP3 inflammasome-related proteins in *si-Kv2.1*-treated microglia (n = 3). (J) Immunofluorescence assay and (K) its quantification results

NLRP3 inflammasome in *si-Kv2.1*-treated microglia (Fig. 3H−K). All results indicated that Dfe suppressed NLRP3 inflammasome activation by inhibiting the Kv2.1 channel.

3.3.3. Dfe suppressed o-Aβ-induced NF-κB activation in microglia by inhibiting the Kv2.1 channel

Given that NF-κB as a key nuclear transcription factor regulates the expressions of NLRP3 inflammasome components of NLRP3 and ASC in the priming process[33], we detected whether Dfe suppressed o-Aβ-mediated upregulation of NLRP3 and ASC protein levels through NF-κB. Western blot and immunofluorescence results indicated that o-Aβ treatment increased p-NF-κB protein level (Fig. 3L and M) and promoted NF-κB nuclear translocation (Fig. 3N and O) in microglia, and Dfe treatment inhibited such o-Aβ-induced effects on NF-κB. Moreover, o-Aβ lost its ability in activating NF-κB and Dfe failed to regulate NF-κB in *si-Kv2.1*-treated microglia (Fig. 3L−O). All results demonstrated that Dfe suppressed o-Aβ-induced NF-κB activation by inhibiting the Kv2.1 channel.

3.3.4. Dfe suppressed o-Aβ-mediated priming process of microglial NLRP3 inflammasome by inhibiting the NF-κB

Furthermore, NF-κB inhibitor PDTC (5 μmol/L) was applied in the assay to verify the role of NF-κB in mediating the Dfe-inhibited NLRP3 inflammasome. Western blot results indicated that either Dfe or PDTC treatment antagonized o-Aβ-induced NLRP3 and ASC upregulation, and PDTC blocked the capability of Dfe to regulate these two proteins in microglia (Fig. 3P and Q). Notably, PDTC had no effects on the protein level of p-NLRP3 or Cas1 (p20) (Fig. 3P and Q), indicating that NF-κB was only involved in the priming process of Kv2.1-dependent potassium efflux-mediated NLRP3 inflammasome activation. Therefore, Dfe suppressed the o-Aβ-mediated priming process of microglial NLRP3 inflammasome by inhibiting NF-κB.

3.3.5. Dfe suppressed o-Aβ-induced JNK activation in microglia by inhibiting the Kv2.1 channel

Given that JNK as an intracellular potassium level sensor is stimulated by potassium efflux followed by stimulating NF-κB and phosphorylating NLRP3 to activate NLRP3 inflammasome[33], we investigated whether Dfe suppressed o-Aβ-induced NLRP3 inflammasome by inhibiting JNK. Western blot results (Fig. S4C and S4D) indicated that o-Aβ upregulated p-JNK level and Dfe antagonized the o-Aβ-induced p-JNK upregulation in microglia, while either o-Aβ or Dfe lost its capability in regulating JNK in *si-Kv2.1*-treated microglia. Thus, all results indicated that Dfe suppressed o-Aβ-induced JNK activation through the Kv2.1 channel.

3.3.6. Dfe suppressed o-Aβ induced NLRP3 inflammasome activation through Kv2.1/JNK/NF-κB pathway in brain slices and microglia

Finally, JNK inhibitor SP600125[33] was applied in the assay to investigate the role of JNK in mediating the Dfe-inhibited NLRP3 inflammasome in brain slices and primary microglia. As shown in Fig. S4E−S4H, immunofluorescence and Western blot results indicated that SP600125 treatment abolished the inhibition of Dfe against NLRP3 inflammasome activation and IL-1β release in o-Aβ-treated brain slices. These results thus demonstrated that Dfe suppressed the o-Aβ-induced NLRP3 inflammasome activation in brain slices by inhibiting JNK.

Additionally, Western blot (Fig. S4I and S4J) and immunofluorescence (Fig. S4L and S4M) results indicated that either Dfe or JNK inhibitor SP600125 decreased the levels of NLRP3 inflammasome component proteins (p-NLRP3, NLRP3, ASC and Cas1 (p20)) and the number of NLRP3-ASC positive puncta in Aβ-treated microglia. Notably, Dfe lost its capability to regulate any of the NLRP3 inflammasome component proteins in SP600125-treated microglia (Fig. S4I and S4J; Fig. S4L and S4M).

Moreover, SP600125 deprived either o-Aβ of its agonistic activity or Dfe of its inhibitory activity against NF-κB in microglia (Fig. S4I and S4K), which suggested that o-Aβ-induced Kv2.1-dependent potassium leakage activated NF-κB through regulating JNK.

Thus, all results indicate that Dfe suppressed o-Aβ-induced NLRP3 inflammasome activation by inhibiting Kv2.1/JNK/NF-κB pathway.

3.4. Dfe suppressed microglial NLRP3 inflammasome-driven neuronal tauopathy by inhibiting the Kv2.1 channel

Given that microglial NLRP3 inflammasome links Aβ to tauopathy through matured IL-1β[15], we investigated whether Dfe treatment might block microglial NLRP3 inflammasome-mediated neuronal tau hyperphosphorylation.

AT8 staining assay against brain slices was performed to detect the levels of hyperphosphorylated Tau at sites of Ser202 and Thr205[26]. As shown in Fig. 4A and B, the o-Aβ treatment effectively increased AT8-positive areas in cultured brain slices, while Dfe suppressed o-Aβ-induced Tau hyperphosphorylation in cultured brain slices.

Moreover, the AT8 staining assay against MG-Kv2.1-*KD* brain slices was also performed to further verify the role of microglial Kv2.1 in the Aβ-Tau cascade reaction. As shown in Fig. 4C−E, microglial Kv2.1 specific knockdown suppressed o-Aβ-induced Tau hyperphosphorylation in brain slices, while Dfe had no impacts on Tau hyperphosphorylation in MG-Kv2.1-*KD* brain slices. All results thus indicated that microglial Kv2.1 was mainly responsible for o-Aβ induced Tau hyperphosphorylation and Dfe suppressed such Tau hyperphosphorylation through microglial Kv2.1.

Moreover, to further confirm the inhibition of Dfe against the Aβ-Tau cascade reaction, the conditioned medium was obtained with microglia treated by DMSO, o-Aβ, o-Aβ+Dfe, *si-Kv2.1*, o-

demonstrated that Dfe treatment reduced the number of NLRP3-ASC positive puncta in microglia, and Dfe failed to regulate NLRP3 inflammasome in *si-Kv2.1*-treated microglia. Scale bar: 50 μm ($n = 4$). (L) Western blot assay and (M) its quantification results indicated that Dfe treatment reduced the protein level of p-NF-κB in microglia, and Dfe failed to regulate p-NF-κB level in *si-Kv2.1*-treated microglia ($n = 3$). (N) Immunofluorescence assay and (O) its quantification results demonstrated that Dfe treatment suppressed NF-κB nucleus translocation in microglia, and Dfe failed to regulate NF-κB in *si-Kv2.1*-treated microglia. Scale bar: 50 μm ($n = 4$). (P) Western blot assay and (Q) its quantification results indicated that either Dfe or PDTC treatment suppressed o-Aβ-induced upregulation of NLRP3 and ASC, and PDTC blocked the capability of Dfe in regulating the expressions of these proteins in microglia ($n = 3$). All values are presented as mean ± SEM. ns, not significant; $^{*}P < 0.05$, $^{**}P < 0.01$, $^{***}P < 0.001$ compared by one-way ANOVA test.

Aβ+*si-Kv2.1* or o-Aβ+Dfe+*si-Kv2.1*, and then applied to culture neurons. Additionally, to exclude the effect of residual Dfe in the medium on neurons, the conditioned medium was centrifuged by using concentrator tubes (5 kDa) to remove the compound. Protein levels of Aβ and IL-1β in the medium were detected before the assay. Western blot results indicated that o-Aβ obviously increased the protein level of IL-1β in medium from microglia and Dfe effectively suppressed o-Aβ-induced IL-1β releasing from microglia (Fig. 4F and G). No residual Aβ was detected in the medium from microglia (Supporting Information Fig. S5A), indicating that the exogenous Aβ has been completely devoured by microglia after 6 h incubation and the neuron would not be affected by residual Aβ in the medium from microglia.

Western blot assay was performed to detect the protein levels of tau phosphorylation at sites of Ser396, Ser231, and Thr199 in neurons incubated with conditioned medium (Fig. 4H and I). As far as the compositions of the conditioned medium are concerned, Dfe treatment antagonized the o-Aβ-induced upregulation of neuronal tau phosphorylation (p^{396}-Tau, p^{231}-Tau, and p^{199}-Tau) and *si-Kv2.1* treatment deprived Dfe of its antagonistic activity against tau hyperphosphorylation (Fig. 4H and I). In addition, results of the immunofluorescence assay against AT8 also indicated that Dfe treatment suppressed the o-Aβ-treated microglial conditioned medium-induced Tau hyperphosphorylation in neurons (Fig. 4J and K).

Moreover, two kinases GSK3β and CaMKII-α that are responsible for tau phosphorylation were also detected by Western blot assay. As shown in Fig. 4L and M, Dfe treatment antagonized the o-Aβ-treated microglial conditioned medium-induced upregulations of p-GSK3β and p-CaMKII-α in neurons, and *si-Kv2.1* deprived Dfe of its antagonistic activity against these two kinases.

Thus, all results indicated that Dfe suppressed microglial NLRP3 inflammasome-driven neuronal tauopathy by inhibiting the Kv2.1 channel.

3.5. Dfe suppressed o-Aβ induced neuronal apoptosis by inhibiting the Kv2.1 channel

Given that the Kv2.1 inhibitor exhibits neuroprotective effects in central system diseases such as stroke and cerebral ischemia[34] and o-Aβ can induce neuronal apoptosis[35], we investigated whether Dfe suppressed o-Aβ-induced neuronal apoptosis by inhibiting the Kv2.1 channel. As shown in Fig. S5B and S5C, the o-Aβ treatment effectively increased the TUNEL-positive areas in cultured brain slices, while Dfe suppressed o-Aβ-induced neuronal apoptosis in MG-Kv2.1-*NC* brain slices. Notably, microglial Kv2.1 specific knockdown suppressed o-Aβ-induced neuronal apoptosis on brain slices, while Dfe exhibited still neuroprotective effects by comparing (o-Aβ+Dfe)-treated to o-Aβ-treated groups in MG-Kv2.1-*KD* brain slices (Fig. S5B and S5C). All results thus indicated that microglial Kv2.1 played a partial role in o-Aβ-induced neuronal apoptosis and the Kv2.1 antagonism of Dfe on neurons might be involved in its anti-apoptotic effect.

In the following assay, we at first detected the effect of o-Aβ on intracellular potassium levels of neurons by using potassium probe EPG-4. As shown in Fig. S5D and S5E, o-Aβ reduced intracellular potassium levels in neurons and Dfe treatment antagonized the o-Aβ-induced downregulation of neuronal intracellular potassium level. Notably, Dfe failed to regulate neuronal potassium levels in *si-Kv2.1*-treated neurons, indicating that Dfe suppressed o-Aβ induced neuronal potassium efflux by inhibiting the Kv2.1 channel.

Furthermore, Western blot and flow cytometry results indicated that Dfe inhibited o-Aβ-induced upregulation of mitochondrial apoptosis-related proteins[36] (Bax and cleaved-Cas3, Fig. S5F and S5G) and apoptosis (Fig. S5H) in neurons, while *si-Kv2.1* deprived Dfe of its above-mentioned inhibitory activities. These results thus demonstrated that Dfe suppressed o-Aβ-induced neuronal apoptosis by inhibiting the Kv2.1 channel.

3.6. Dfe ameliorated cognitive impairment of 5×FAD-AD mice by targeting Kv2.1 channel

Next, we inspected the potential of Dfe in ameliorating memory and cognitive impairment of female and male 5×FAD-AD mice by assays of NOR, Y-maze, and MWM. In the assay, Dfe treatment (10 mg/kg/day, intraperitoneal injection) or selective Kv2.1 knockdown in the brain by tail vein injecting AAV-*si-Kv2.1* was performed in mice experiments (Fig. 5A). The knockdown efficiency of AAV-*si-Kv2.1* against cerebral Kv2.1 and microglial Kv2.1 were shown in Supporting Information Fig. S6A−S6E.

3.6.1. NOR test

The test was performed to evaluate the amelioration of Dfe on short-term working memory of 5×FAD-AD mice. As shown in Fig. 5B (male, Fig. S6G), 5×FAD-AD mice spent less time around the new object compared with WT mice, while treatment of Dfe increased the time spent around the new object for 5×FAD-AD mice, thus indicating that Dfe ameliorated short-term working memory impairment of 5×FAD-AD mice.

3.6.2. Y-maze test

This test was used to assess the amelioration of Dfe on spatial working memory. As indicated in Fig. 5D (male, Fig. S6I), the number of crossing new arm for 5×FAD-AD mice was more than that for WT mice, and treatment of Dfe increased the number of crossing new arm for 5×FAD-AD mice. These results thereby indicate that Dfe ameliorated spatial working memory impairment of 5×FAD-AD mice.

3.6.3. MWM test

This test was used to assess the amelioration of Dfe on spatial learning and long-term memory of 5×FAD-AD mice. As indicated in Fig. 5F and H (male, Fig. S6K and S6M), 5×FAD-AD mice spent more time reaching the platform and crossed the target quadrant with less frequency than WT mice, and Dfe treatment decreased the time spent in reaching the platform and increased the frequency in crossing the target quadrant for 5×FAD-AD mice. These results thus demonstrate that Dfe ameliorated spatial learning and long-term memory impairments of 5×FAD-AD mice.

Notably, Dfe treatment failed to ameliorate any of the above-mentioned pathological behaviors in AAV-*si-Kv2.1* injected 5×FAD-AD mice (female, Fig. 5C, E, G and I; male, Fig. S6H, S6J, S6L and S6N).

Moreover, the hepatotoxicity and nephrotoxicity of Dfe treatment (10 mg/kg) on female mice were evaluated by detecting the levels of ALT, AST and Urea in serum, and the results indicated that Dfe treatment (10 mg/kg) exhibited no obvious toxicities on either WT mice or 5×FAD mice (female, Fig. S6O−S6Q).

Together, Dfe ameliorated cognitive impairment of 5×FAD-AD mice by inhibiting the Kv2.1 channel.

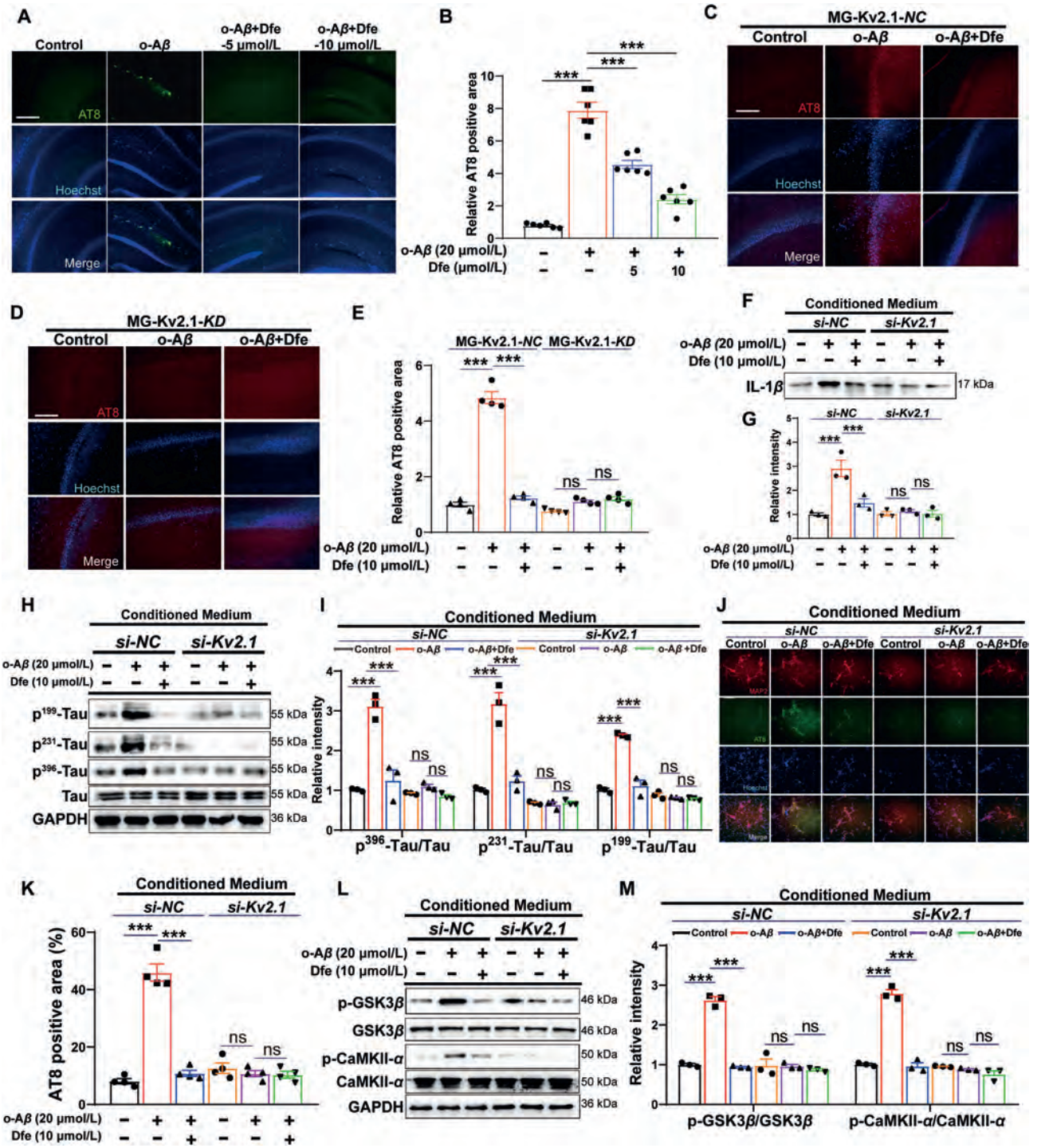

Figure 4 Dfe suppressed microglial NLRP3 inflammasome activation-driven neuronal tauopathy by inhibiting the Kv2.1 channel. (A) Immunofluorescence assay and (B) its quantification results demonstrated that Dfe treatment reduced the AT8-positive areas in o-Aβ-treated brain slices. Scale bar: 100 μm ($n = 6$). (C, D) Immunofluorescence assay and (E) its quantification results demonstrated that Dfe treatment reduced the AT8-positive areas in brain slices and Dfe had no impacts on AT8-positive areas in MG-Kv2.1-*KD* brain slices. Scale bar: 200 μm ($n = 4$). (F, H) Western blot assay and (G, I) its quantification results indicated that Dfe treatment reduced the level of IL-1β in medium from o-Aβ-treated microglia and suppressed o-Aβ-treated microglial conditioned medium-induced neuronal Tau hyperphosphorylation at the site of Ser396, Ser231, and Thr199 ($n = 3$). (J) Immunofluorescence assay and (K) its quantification results demonstrated that Dfe treatment suppressed o-Aβ-treated microglial conditioned medium-induced neuronal Tau hyperphosphorylation. Scale bar: 100 μm ($n = 4$). (L) Western blot assay and (M) its quantification results demonstrated that Dfe treatment suppressed o-Aβ-treated microglial conditioned medium-upregulated p-GSK3β and p-CaMKII-α levels ($n = 3$). All values are presented as mean ± SEM. ns, not significant; $^*P < 0.05$, $^{**}P < 0.01$, $^{***}P < 0.001$ compared by one-way ANOVA test.

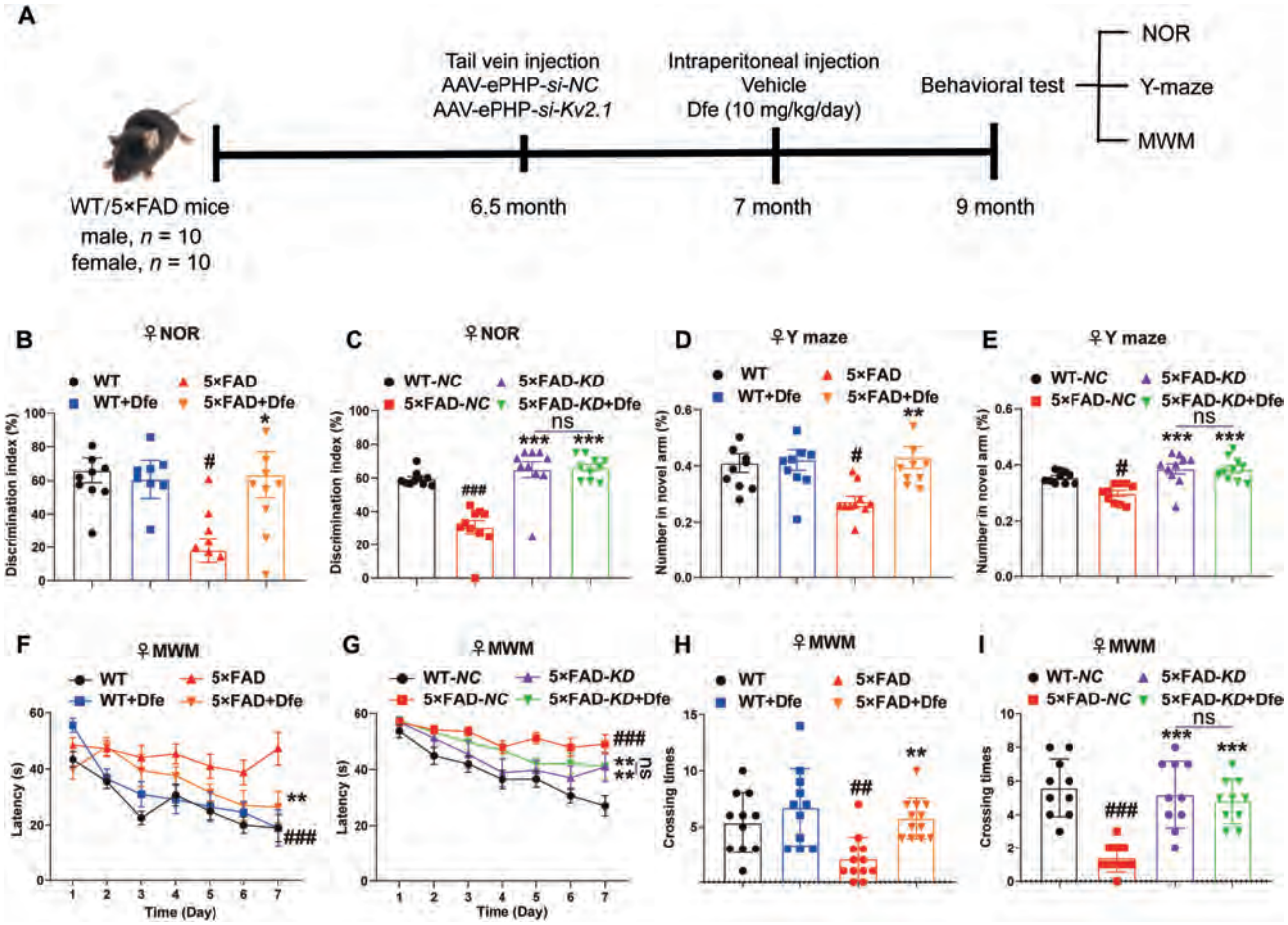

Figure 5 Dfe ameliorated cognitive impairment of 5×FAD-AD mice by targeting the Kv2.1 channel. (A) Schedule of animal treatments and behavior tests against (female and male) WT and 5×FAD-AD mice. 5×FAD-AD mice were treated with Dfe (10 mg/kg/day) at the age of seven months or injected with AAV-ePHP-*si-Kv2.1* through tail vein injection at the age of six and a half months. Animal experiments were performed at the age of nine months of 5×FAD-AD mice. (B, C) NOR test results indicated that Dfe treatment ameliorated short-term working memory defect in female 5×FAD-AD mice, and Dfe failed to improve short-term working memory defect in female 5×FAD-*KD* mice ($n = 10$). (D, E) Y-maze test results indicated that Dfe treatment ameliorated short-term spatial working memory defect in female 5×FAD-AD mice, and Dfe treatment failed to improve short-term spatial working memory defect in female 5×FAD-*KD* mice ($n = 10$). (F, G) Escape latency results during platform trials in the MWM test indicated that Dfe treatment ameliorated learning and memory defects in female 5×FAD-AD mice, and Dfe treatment failed to improve the learning and memory defects in female 5×FAD-*KD* mice ($n = 10$). (H, I) Times of platform crossing in probe trials of the MWM test indicated that Dfe treatment ameliorated the long-term memory defects in female 5×FAD-AD mice, and Dfe treatment failed to improve the long-term memory defects in female 5×FAD-*KD* mice ($n = 10$). All values are presented as mean ± SEM. ns, not significant; $^{\#}P < 0.05$, $^{\#\#}P < 0.01$, $^{\#\#\#}P < 0.001$ compared with WT or WT-*NC* mice by two-way ANOVA test; $^{*}P < 0.05$, $^{**}P < 0.01$, $^{***}P < 0.001$ compared with 5×FAD or 5×FAD-*NC* mice by two-way ANOVA test.

3.7. Dfe suppressed NLRP3 inflammasome activation in 5×FAD-AD mice through Kv2.1/JNK/NF-κB pathway

As indicated in the published reports, the abundance of preclinical and clinical evidence suggests an increase in intrinsic AD risk for women and the AD-related symptoms of female patients are severer than those of male patients[37,38], while the female 5×FAD mice exhibit a more aggressive amyloid pathology compared to male mice[39], we focused on confirming the potential mechanisms of Dfe against NLRP3 activation in brain of female 5×FAD-AD mice (abbreviated as 5×FAD-AD mice).

3.7.1. Dfe suppressed gliosis in the brain of 5×FAD-AD mice

Considering that gliosis is an important marker of inflammatory response in CNS[40], the effect of Dfe on gliosis in the brain of 5×FAD-AD mice was detected by immunofluorescence assay against IBa1 (for microglia) and GFAP (for astrocyte). As shown in Fig. 6A–C, there was a large number of IBa1 (microglia)/GFAP (astrocyte)-positive areas in the brain of 5×FAD-AD mice compared with those in the brain of WT mice, while Dfe treatment reduced the IBa1 (microglia)/GFAP (astrocyte)-positive areas in 5×FAD-AD mice. All these results indicate that Dfe suppressed gliosis in the brain of 5×FAD-AD mice.

3.7.2. Dfe suppressed NLRP3 inflammasome activation in 5×FAD-AD mice

Immunofluorescence and Western blot results indicated that Dfe treatment effectively reduced the numbers of NLRP3-ASC positive puncta in the hippocampus (Fig. 6D and E) and repressed the protein levels of NLPR3, p-NLRP3, ASC, Cas1 (p20) and IL-1β in brains (Fig. 6G and H) of 5×FAD-AD mice.

3.7.3. Dfe suppressed NLRP3 inflammasome activation in 5×FAD-AD mice through JNK/NF-κB pathway

As we have determined that Dfe suppressed NLRP3 inflammasome activation through JNK/NF-κB pathway *in vitro*, we next verified the regulation of Dfe against this pathway in 5×FAD-AD mice.

Western blot (Fig. 6G and H) and immunofluorescence (Fig. 6J and K) results indicate that Dfe treatment effectively reduced the protein levels of p-JNK and p-NF-κB and microglial nuclear translocation of NF-κB (hippocampal microglia were labeled by IBa1 antibody) in the brain of 5×FAD-AD mice. Notably, Dfe had no impacts on NLRP3 inflammasome or JNK/NF-κB pathway in AAV-*si-Kv2.1* injected 5×FAD-AD mice (Fig. 6), indicating that Dfe suppressed NLRP3 inflammasome activation in 5×FAD-AD mice through Kv2.1/JNK/NF-κB pathway.

Moreover, immunofluorescence results (Supporting Information Fig. S7A and S7B) indicated that Dfe treatment had no effects on Aβ level in the hippocampus of 5×FAD-AD mice. These results thus excluded the involvement of Aβ level regulation in Dfe-mediated NLRP3 inflammasome suppression.

Furthermore, to verify the Dfe-mediated regulation of JNK against Aβ/Kv2.1/NLRP3 axis, the effects of Dfe on other potassium ion sensing-related pathways including NEK7, a downstream responsive protein of the potassium efflux involved in NLRP3 activation[41]; ERK, a key apoptotic factor in potassium deprivation-induced neuronal cell death[42]; CaMKK2, a Ca^{2+}/CaM-dependent protein kinase kinase activated by Kv2.1 inhibition[43] and NLRP3 activation-related pathway (TXNIP, a multiprotein complex that promotes the assembly of NLRP3 inflammasomes[44]) were detected in the brain of 5×FAD-AD mice. As shown in Fig. S7C and S7D, Dfe failed to regulate the protein levels of NEK7, TXNIP, p-CaMKK2, and p-ERK in the brain of 5×FAD-AD mice, which thus supported that the JNK pathway suppression mediated by Dfe was involved in the inhibition of Kv2.1 against Aβ-mediated NLRP3 activation.

Together, Dfe suppressed NLRP3 inflammasome activation in 5×FAD-AD mice through Kv2.1/JNK/NF-κB pathway.

3.8. Dfe suppressed Aβ-mediated tauopathy in 5×FAD-AD mice by targeting the Kv2.1 channel

Considering that tauopathy as the terminal effector of Aβ-Tau cascade reaction is key to nerve damage[45], an AT8 staining assay was performed to detect the levels of hyperphosphorylated Tau at sites of Ser202 and Thr205 in hippocampus of 5×FAD-AD mice, and the results indicate that Dfe treatment reduced the levels of hyperphosphorylated Tau at both sites in brain of 5×FAD-AD mice (Fig. 7A and B).

Next, a Western blot assay was performed, and the results indicated that Dfe treatment reduced the protein levels of p^{396}-Tau, p^{231}-Tau, and p^{199}-Tau in the brains of 5×FAD-AD mice (Fig. 7D and E).

Moreover, the effects of Dfe on Tau phosphorylation kinases GSK3β and CaMKII-α in the brain of 5×FAD-AD mice were also detected. Western blot results demonstrate that Dfe treatment reduced the protein levels of p-GSK3β and p-CaMKII-α (Fig. 7D–F).

Notably, Dfe had no impacts on the levels of p-Tau at any above-mentioned sites, p-GSK3β or p-CaMKII-α in AAV-*si-Kv2.1* injected 5×FAD-AD mice as indicated by AT8 staining and Western blot results (Fig. 7A, C, D and F).

Together, all results demonstrate that Dfe suppressed Aβ-mediated tauopathy in 5×FAD-AD mice by inhibiting the Kv2.1 channel.

3.9. Dfe improved synaptic impairment and neuronal loss in 5×FAD-AD mice by targeting the Kv2.1 channel

Given that neuronal synaptic function is responsible for the formation and development of cognitive memory and Aβ/Tau pathology-mediated neurotoxicity directly damages synaptic function[46], we further investigated the potential effect of Dfe on synaptic protection in 5×FAD-AD mice.

3.9.1. Dfe improved synaptic impairment in 5×FAD-AD mice by inhibiting the Kv2.1 channel

The long-term potentiation (LTP) result indicated that Dfe treatment improved LTP induction and maintenance in hippocampal DG region of 5×FAD-AD mice (Fig. 8A). Western blot (Fig. 8C and D) and immunofluorescence (Fig. 8F and G) results demonstrate that Dfe treatment reversed the deficiency of synaptic associated proteins PSD95, VAMP2, and synaptophysin (SYN) in brains of 5×FAD-AD mice.

Notably, the results of LTP (Fig. 8B), Western blot (Fig. 8C and E) and immunofluorescence (Fig. 8F and H) all demonstrate that Dfe had no impacts on the regulation of LTP or any of the synapse-associated proteins in AAV-*si-Kv2.1* injected 5×FAD-AD mice, thus indicating that Dfe improved synaptic impairment in 5×FAD-AD mice by inhibiting the Kv2.1 channel.

3.9.2. Dfe improved neuronal loss in 5×FAD-AD mice by inhibiting the Kv2.1 channel

Additionally, given that neurons are parenchymal cells in memory formation, the effect of Dfe on neuronal loss in the brain of 5×FAD-AD mice were detected by TUNEL and Nissl staining assays. TUNEL staining results (Fig. 8I and J) indicate that there was a large number of TUNEL puncta in the brain of 5×FAD-AD mice compared with those in WT mice, while Dfe treatment reduced the TUNEL puncta in 5×FAD-AD mice. Additionally, Nissl staining results (Fig. 8L) also demonstrate that the neuronal nuclear in the brain of 5×FAD-AD mice were loosely arranged, while Dfe treatment reversed this pathological change in 5×FAD-AD mice, indicating that Dfe suppressed neuronal loss in 5×FAD-AD mice.

Notably, TUNEL and Nissl staining results demonstrated that Dfe had no impacts on the regulation of neuronal loss in AAV-*si-Kv2.1* injected 5×FAD-AD mice (Fig. 8I, K and L), indicating that Dfe suppressed neuronal loss in 5×FAD-AD mice by inhibiting the Kv2.1 channel.

Therefore, all results indicate that Dfe improved synaptic impairment and neuronal loss in 5×FAD-AD mice by inhibiting the Kv2.1 channel.

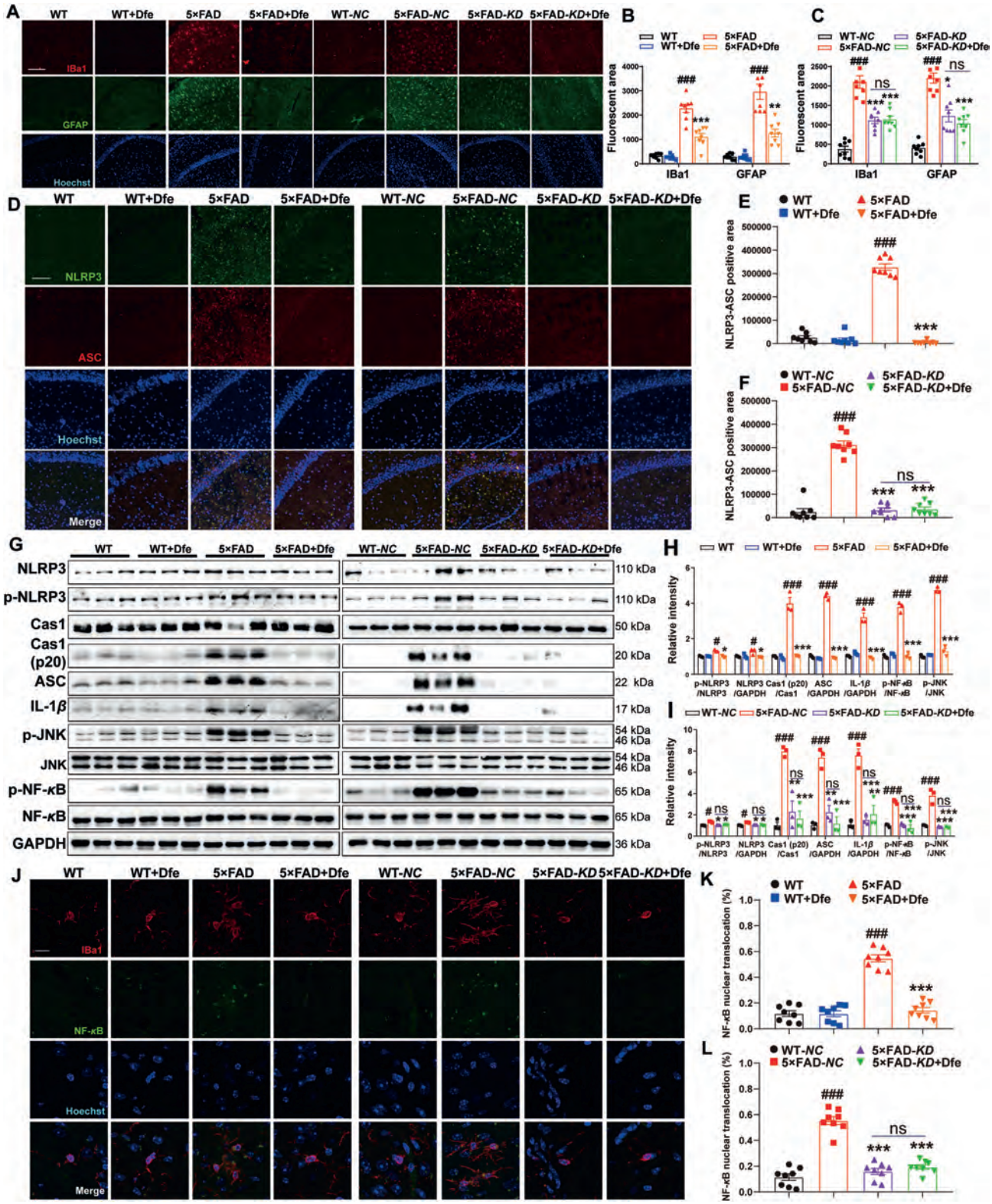

Figure 6 Dfe suppressed NLRP3 inflammasome activation in 5×FAD-AD mice through Kv2.1/JNK/NF-κB pathway. (A) Immunofluorescence assay and (B, C) its quantification results demonstrated that Dfe treatment suppressed gliosis in the brains of 5×FAD-AD mice, and Dfe treatment failed to suppress gliosis in the brain of 5×FAD-*KD* mice. Scale bar: 200 μm ($n = 8$). (D) Immunofluorescence assay and (E, F) its quantification results demonstrated that Dfe treatment suppressed NLRP3 inflammasome activation in the brain of 5×FAD-AD mice, and Dfe treatment failed to suppress NLRP3 inflammasome activation in the brain of 5×FAD-*KD* mice. Scale bar: 150 μm ($n = 8$). (G) Western blot assay and (H, I) its quantification results indicated that Dfe treatment suppressed NLRP3 inflammasome activation in the brain of 5×FAD-AD mice, and Dfe treatment failed to suppress NLRP3 inflammasome activation in the brain of 5×FAD-*KD* mice ($n = 3$). (J) Immunofluorescence assay and (K, L)

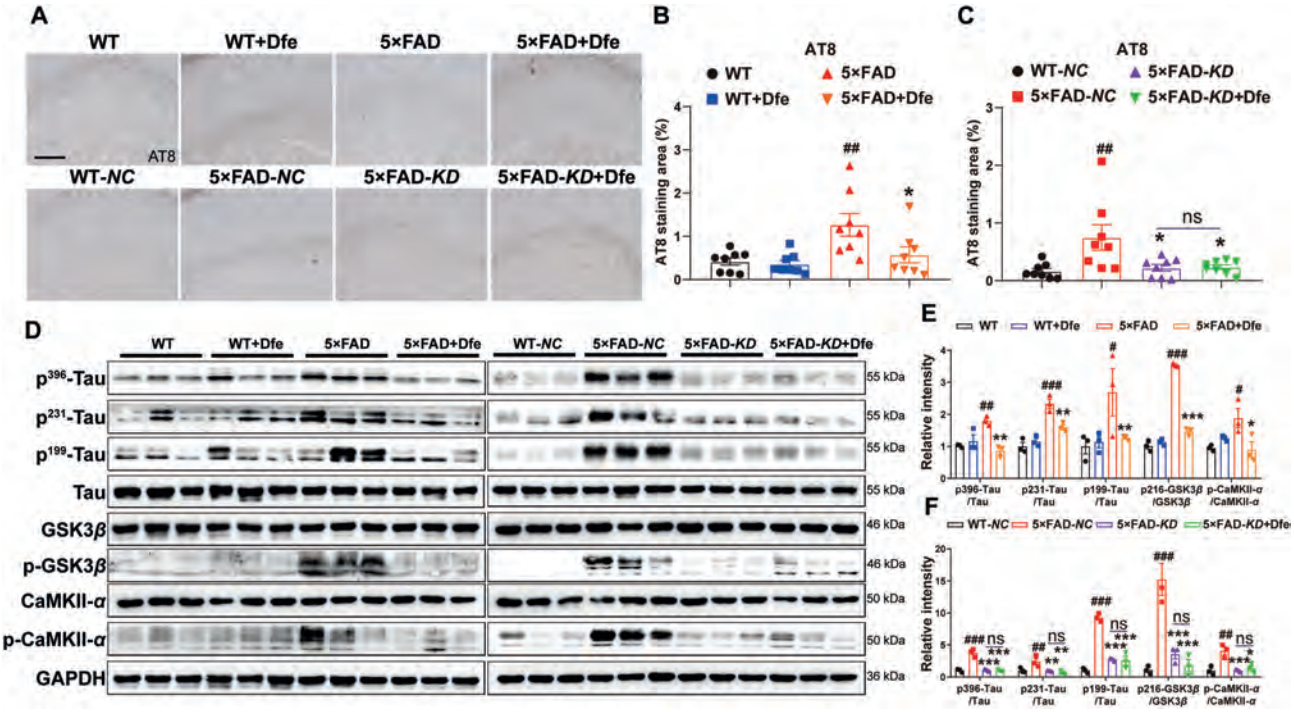

Figure 7 Dfe suppressed Aβ-mediated tauopathy in 5×FAD-AD mice by targeting the Kv2.1 channel. (A) AT8 staining assay and (B, C) its quantification results demonstrated that Dfe treatment suppressed AT8 positive areas in the hippocampus of 5×FAD-AD mice, and Dfe treatment failed to suppress tauopathy in the hippocampus of 5×FAD-*KD* mice. Scale bar: 200 μm ($n = 8$). (D) Western blot assay and (E, F) its quantification results indicated that Dfe treatment suppressed Tau hyperphosphorylation (p^{396}-Tau, p^{231}-Tau and p^{199}-Tau) and related kinases (GSK3β and CaMKII-α) in brain of 5×FAD-*KD* mice, and Dfe treatment failed to suppress Tau hyperphosphorylation (p^{396}-Tau, p^{231}-Tau and p^{199}-Tau) and related kinases (GSK3β and CaMKII-α) in 5×FAD-*KD* mice ($n = 3$). All values are presented as mean ± SEM. ns, not significant; $^{\#}P < 0.05$, $^{\#\#}P < 0.01$, $^{\#\#\#}P < 0.001$ compared with WT or WT-*NC* mice by two-way ANOVA test; $^{*}P < 0.05$, $^{**}P < 0.01$, $^{***}P < 0.001$ compared with 5×FAD or 5×FAD-*NC* mice by two-way ANOVA test.

4. Discussion

The Aβ-Tau cascade reaction hypothesis is one of the mainstream theories on the pathogenesis of AD. It is believed that Aβ as one of the earliest pathological features is responsible for the initiation of the Aβ-Tau cascade reaction in the brains of AD patients[7,47]. Recent studies have also shown that microglial NLRP3 inflammasome activation is a key link connecting Aβ with neuronal tauopathy in AD mice[15], although the underlying mechanism for Aβ driving NLRP3 inflammasome activation is not yet clear. Notably, many studies have ever attempted to interpret this mechanism from the perspective of Aβ intracellular influences such as mitochondria or endoplasmic reticulum damage while ignoring the effect of Aβ on ion channels from cell membranes. Here, we determined that o-Aβ promoted microglial potassium efflux through the Kv2.1 channel leading to NLRP3 inflammasome activation and further neuronal tauopathy. Moreover, we further verified such a finding by using our previously determined Kv2.1 inhibitor Dfe[17] as a probe, and we found that Dfe treatment had no effects on Aβ regulation but efficiently alleviated AD-like pathology in 5×FAD-AD mice *via* blocking Aβ-Tau cascade reaction. Our findings have strongly provided new evidence that the Kv2.1 channel is required for Aβ-driven NLRP3 inflammasome activation and further Tau hyperphosphorylation and highly addressed Kv2.1 inhibitor Dfe may show promise as a lead compound for AD treatment.

In the current work, we reported that the microglial Kv2.1 channel was obviously upregulated and enormously co-localized with Aβ in the brains of 5×FAD-AD mice, while there was no such an event in other cells including neurons and astrocytes. Moreover, we found that o-Aβ stimulated microglial potassium efflux through binding to the Kv2.1 channel. We suspected that the chemotactic function of microglia was responsible for its specific Kv2.1 upregulation. In AD pathology, microglia actively recognize and approach Aβ, followed by phagocytosis[48]. This process made microglia more adversely affected by Aβ than other cells and Aβ readily bound to microglial Kv2.1 to mediate its potassium efflux. Notably, this may be also the reason why microglia are often the first cell population to exhibit pathological responses during AD development.

In the current study, we found that Aβ could induce microglial potassium efflux by directly binding to the Kv2.1 channel, while

its quantification results demonstrated that Dfe treatment suppressed NF-κB nucleus translocation in the hippocampus of 5×FAD-AD mice, and Dfe treatment failed to regulate NF-κB nucleus translocation in the hippocampus of 5×FAD-*KD* mice. Scale bar: 50 μm ($n = 8$). All values are presented as mean ± SEM. ns, not significant; $^{\#\#}P < 0.01$, $^{\#\#\#}P < 0.001$ compared with WT or WT-*NC* mice by two-way ANOVA test; $^{*}P < 0.05$, $^{**}P < 0.01$, $^{***}P < 0.001$ compared with 5×FAD or 5×FAD-*NC* mice by two-way ANOVA test.

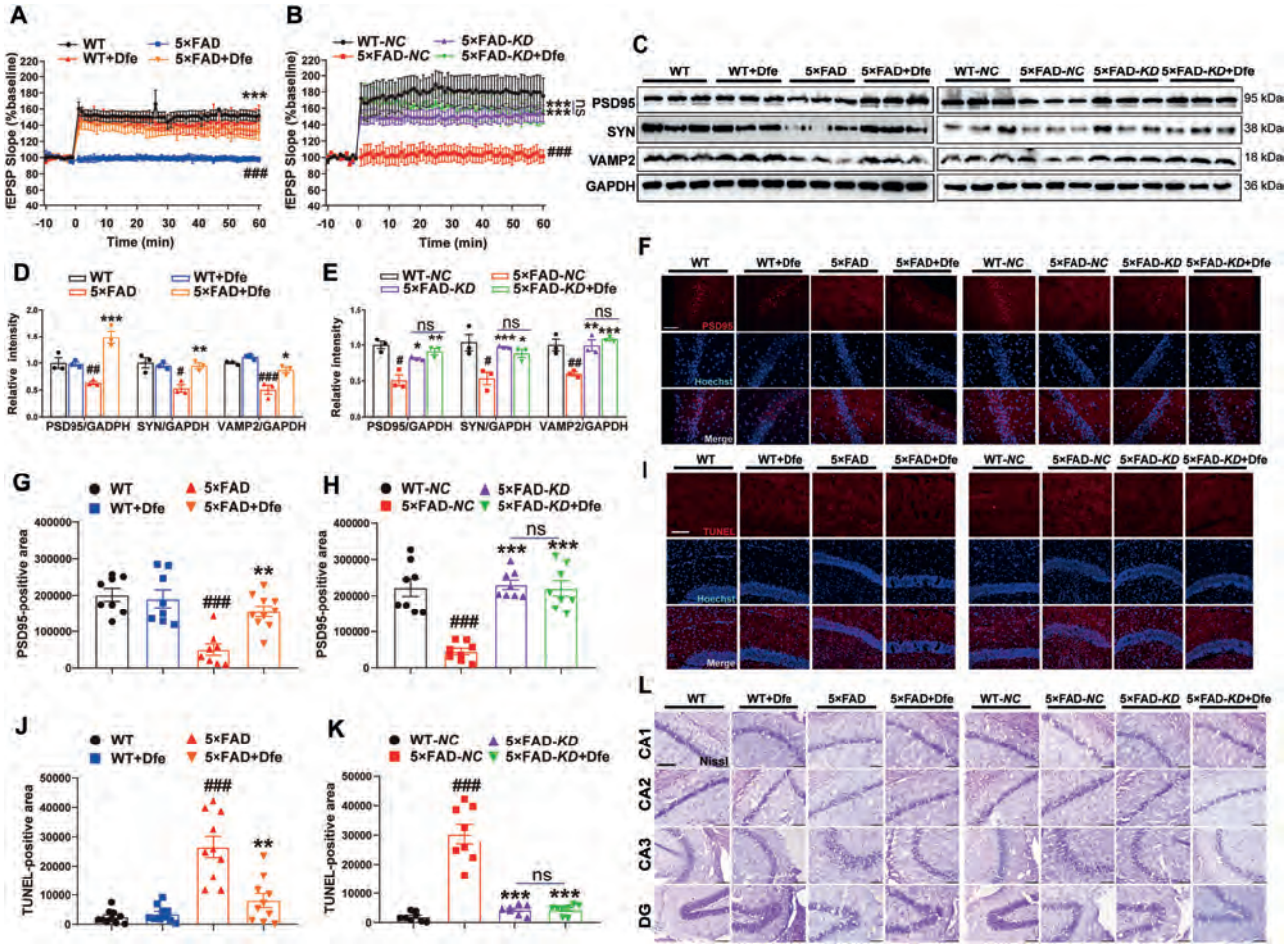

Figure 8 Dfe improved synaptic impairment and neuronal loss in 5×FAD-AD mice by targeting the Kv2.1 channel. (A, B) Electrophysiology assay results indicated that Dfe treatment upregulated summary plots of mean normalized fEPSP slope after HFS (4×100 Hz) in the hippocampus (DG region) of 5×FAD-AD mice, while Dfe treatment failed to regulate LTP in the hippocampus (DG region) of 5×FAD-*KD* mice ($n = 6$). (C) Western blot assay and (D, E) its quantification results demonstrated that Dfe treatment reversed synaptic proteins (PSD95, SYN, and VAMP2) defects in the brain of 5×FAD-AD mice, and Dfe treatment failed to regulate these synaptic protein levels in 5×FAD-*KD* mice ($n = 3$). (F) Immunofluorescence assay and (G, H) its quantification results demonstrated that Dfe treatment reversed synaptic protein PSD95 defect in the hippocampus of 5×FAD-AD mice, and Dfe treatment failed to regulate protein level of PSD95 in the hippocampus of 5×FAD-*KD* mice. Scale bar: 100 μm ($n = 8$). (I) TUNEL staining assay and (J, K) its quantification results demonstrated that Dfe treatment suppressed neuronal apoptosis in the hippocampus of 5×FAD-AD mice, and Dfe treatment failed to regulate neuronal apoptosis in the hippocampus of 5×FAD-*KD* mice. Scale bar: 200 μm ($n = 8$). (L) Nissl staining results demonstrated that Dfe treatment suppressed neuronal loss in the hippocampus of 5×FAD-AD mice, and Dfe treatment failed to regulate neuronal loss in the hippocampus of 5×FAD-*KD* mice. Scale bar: 200 μm ($n = 6$). All values are presented as mean ± SEM. ns, not significant; $^{\#\#}P < 0.01$, $^{\#\#\#}P < 0.001$ compared with WT or WT-*NC* mice by two-way ANOVA test; $^{*}P < 0.05$, $^{**}P < 0.01$, $^{***}P < 0.001$ compared with 5×FAD or 5×FAD-*NC* mice by two-way ANOVA test.

Dfe effectively abolished such an effect of o-Aβ on potassium current. Due to the structural complexity of o-Aβ, it is extremely difficult for us to predict or detect the exact binding site of o-Aβ and the Kv2.1 channel. Interestingly, kinetic (activation/inactivation) assays against Kv2.1 channel results indicate that o-Aβ had no effects on the activation of the Kv2.1 channel but delayed the inactivation of the Kv2.1 channel, while Dfe has the same effect as o-Aβ on Kv2.1 activation/inactivation state and offsets such an ability of o-Aβ. In our previous study, we reported that Dfe as a Kv2.1 inhibitor blocked the Kv2.1 channel-dependent potassium current[17], and was supposed to bind to the sites in the pore domains (S5 and S6) of the Kv2.1 channel. Herein, we speculated that o-Aβ with a large molecular weight might bind to the sites S1−S4[28] in the voltage-sensor domain of the Kv2.1 channel followed by upregulation of potassium efflux, which was suppressed by Dfe as a non-competitive inhibitor of Kv2.1 channel.

Herein, we found that Kv2.1 expression was mainly increased in microglia and slightly increased in neurons, but unchangeable in astrocytes of the brain of 5×FAD-AD mice. We speculated that the location of o-Aβ was responsible for the differences in Kv2.1 expression among these cell populations. In our study, we determined that o-Aβ was able to directly combine and stabilize Kv2.1 in the brain of 5×FAD-AD mice. In that case, the Kv2.1 channel from neurons can conditionally interact with surrounding o-Aβ[49] and be slightly upregulated. Notably, microglia as immune cells in the brain greatly trend towards o-Aβ and enormously co-locate

with o-Aβ[50]. Therefore, among the multiple cell populations in the brain, microglia were one of the major cell populations disturbed by Aβ thus resulting in significant upregulation of Kv2.1.

NLRP3 inflammasome activation requires priming and assembly processes. In the priming process, the expressions of NLRP3 inflammasome components including NLRP3 and ASC are upregulated[33], and in the assembly process, these components are assembled into an active complex NLRP3 inflammasome resulting in the cleavage of pro-IL-1β into mature IL-1β[15]. Intracellular potassium efflux is generally recognized as one of the pathways for NLRP3 inflammasome activation[40]. Here, we conducted an in-depth investigation of the underlying mechanism for potassium efflux-mediated NLRP3 activation. It was previously reported that JNK as a sensor of cellular potassium efflux participates in cell apoptosis progress[51]. We found that JNK activation induced by Aβ-mediated Kv2.1-dependent potassium efflux was responsible for both microglial NLRP3 inflammasome priming and assembly processes, in that JNK activates NF-κB and promotes its nuclear translocation leading to upregulation of NLRP3 inflammasome components NLRP3 and ASC, while JNK simultaneously phosphorylates NLRP3 at Ser194 site and stimulates assembly of NLRP3 inflammasome. To our knowledge, our present work might be the first to reveal the key role of JNK in the combination of both priming and assembly processes for NLRP3 inflammasome activation.

Microglia as the main immune cells in the brain are sensitively activated by Aβ with the release of a series of inflammatory factors such as IL-1β, TNF-α, and iNOS[52]. Among these inflammatory factors, IL-1β functions as a major mediator responsible for microglial inflammation-induced neuronal tauopathy that directly damages neurons. Regrettably, several reagents or monoclonal antibodies targeting Tau such as LMTX (TauRx Therapeutics)[9] and Gosuranemab[3] (Biogen) failed in clinical trials, demonstrating the complexity of AD pathology. Here, we determined that the Kv2.1 channel is a key linking o-Aβ to the NLRP3/Tau axis, and Dfe treatment blocks the capability of o-Aβ in activating NLRP3 inflammasome activation and subsequent neuroinflammation and tau hyperphosphorylation. Our study highly addressed the potency of the Kv2.1 channel in mediating the Aβ-Tau cascade reaction involving the crosstalk between microglia and neurons.

Notably, the Kv2.1 channel is widely expressed in the central nervous system and is one of the main components of delayed rectifier potassium current in neurons[18]. It has been reported that Kv2.1 inhibitor cpd5 exhibited beneficial effects on neurological diseases including stork[53,54]. Here, we confirmed that o-Aβ can induce Kv2.1-dependent potassium efflux followed by neuronal apoptosis, and Dfe as a Kv2.1 inhibitor suppressed o-Aβ-induced neuronal apoptosis by inhibiting the potassium efflux. Our results have well explained the mechanism underlying the Aβ-induced nerve damage and Kv2.1 inhibitor-mediated neuroprotective effects. Notably, we found that no differences exist in the impact of Dfe on the cognition-related behaviors between female and male 5×FAD-AD mice. We tentatively ascribed such a gender-neutral benefit of Dfe to the subtle differential expression of Kv2.1 in brain tissues between female and male 5×FAD-AD mice (Fig. S7E and S7F). These results thus consolidate the universality of Dfe as a Kv2.1 inhibitor in treating AD patients of both genders.

Moreover, Dfe was ever reported to be a butyrylcholinesterase inhibitor and is used clinically as an antispasmodic drug[55]. Its already-known clinical information such as metabolism, toxicity, and pharmacokinetics may help greatly reduce the cost and time of the research and development for anti-AD reagents based on Dfe as an available "old" drug.

5. Conclusions

We determined that o-Aβ induced Kv2.1-dependent potassium efflux leading to the activation of the JNK/NF-κB pathway, followed by stimulation of both priming and assembly processes for NLRP3 inflammasome activation and neuronal tauopathy. Kv2.1 inhibitor Dfe effectively suppressed the o-Aβ-induced microglial NLRP3 inflammasome activation and neuronal Tau hyperphosphorylation by inhibiting Kv2.1/JNK/NF-κB pathway, while improving the cognitive impairment of 5×FAD-AD mice. Our work has highly addressed that microglial Kv2.1-dependent potassium efflux is required for o-Aβ-induced NLRP3 inflammasome activation and tauopathy in AD mice and highlighted that Kv2.1 inhibition shows promise as a therapeutic strategy for AD and Dfe as a Kv2.1 inhibitor shows potential in treating this disease.

Acknowledgments

This work was supported by the National Natural Science Foundation for Young Scientists of China (82404629), the National Natural Science Foundation of China (82473982), the National Key R&D Program of China (2023YFC2308200), the Innovation Projects of State Key Laboratory on Technologies for Chinese Medicine Pharmaceutical Process Control and Intelligent Manufacture (NZYSKL240110, China), the Natural Science Foundation of Jiangsu Province (BK20240729, China), the Major Program of the Natural Science Foundation of the Jiangsu Higher Education Institutions of China (23KJA350002), the Jiangsu Province Science and Technology Project of Traditional Chinese Medicine (ZT202109, China), the Jiangsu Provincial Medical Innovation Center (CXZX202225, China) and the "Qing Lan" project.

Author contributions

Jian Lu: Formal analysis, Investigation, Software, Visualization, Writing − original draft. Qian Zhou: Formal analysis, Investigation, Software, Visualization. Danyang Zhu: Formal analysis, Investigation, Software, Visualization, Writing − original draft. Hongkuan Song: Formal analysis, Investigation, Visualization, Writing − original draft. Guojia Xie: Investigation, Methodology. Xuejian Zhao: Investigation, Software, Visualization. Yujie Huang: Investigation, Software, Visualization. Peng Cao: Conceptualization, Project administration, Supervision. Jiaying Wang: Conceptualization, Data curation, Project administration, Supervision. Xu Shen: Conceptualization, Project administration, Supervision, Writing − review & editing.

Conflicts of interest

The authors declare that they have no competing interests.

Appendix A. Supporting information

Supporting information to this article can be found online at https://doi.org/10.1016/j.apsb.2024.11.010.

References

1. Mintun MA, Lo AC, Duggan Evans C, Wessels AM, Ardayfio PA, Andersen SW, et al. Donanemab in early Alzheimer's disease. *N Engl J Med* 2021;**384**:1691−704.
2. Du F, Yu Q, Yan S, Hu G, Lue LF, Walker DG, et al. PINK1 signalling rescues amyloid pathology and mitochondrial dysfunction in Alzheimer's disease. *Brain* 2017;**140**:3233−51.
3. Cummings J, Lee G, Ritter A, Sabbagh M, Zhong K. Alzheimer's disease drug development pipeline: 2019. *Alzheimers Dement (N Y)* 2019;**5**:272−93.
4. Chakraborty S, Lennon JC, Malkaram SA, Zeng Y, Fisher DW, Dong H. Serotonergic system, cognition, and BPSD in Alzheimer's disease. *Neurosci Lett* 2019;**704**:36−44.
5. Zhang W, Xu C, Sun J, Shen HM, Wang J, Yang C. Impairment of the autophagy−lysosomal pathway in Alzheimer's diseases: pathogenic mechanisms and therapeutic potential. *Acta Pharm Sin B* 2022;**12**:1019−40.
6. Pascoal TA, Benedet AL, Ashton NJ, Kang MS, Therriault J, Chamoun M, et al. Microglial activation and tau propagate jointly across Braak stages. *Nat Med* 2021;**27**:1592−9.
7. Busche MA, Hyman BT. Synergy between amyloid-β and tau in Alzheimer's disease. *Nat Neurosci* 2020;**23**:1183−93.
8. Luo M, Pang Y, Li J, Yi L, Wu B, Tian Q, et al. miR-429-3p mediates memory decline by targeting MKP-1 to reduce surface GluA1-containing AMPA receptors in a mouse model of Alzheimer's disease. *Acta Pharm Sin B* 2024;**14**:635−52.
9. Congdon EE, Sigurdsson EM. Tau-targeting therapies for Alzheimer disease. *Nat Rev Neurol* 2018;**14**:399−415.
10. Li Y, Yang P, Meng R, Xu S, Zhou L, Qian K, et al. Multidimensional autophagy nano-regulator boosts Alzheimer's disease treatment by improving both extra/intraneuronal homeostasis. *Acta Pharm Sin B* 2024;**14**:1380−99.
11. Bennett RE, Robbins AB, Hu M, Cao X, Betensky RA, Clark T, et al. Tau induces blood vessel abnormalities and angiogenesis-related gene expression in P301L transgenic mice and human Alzheimer's disease. *Proc Natl Acad Sci U S A* 2018;**115**:E1289−98.
12. Yang C, Su C, Iyaswamy A, Krishnamoorthi SK, Zhu Z, Yang S, et al. Celastrol enhances transcription factor EB (TFEB)-mediated autophagy and mitigates Tau pathology: implications for Alzheimer's disease therapy. *Acta Pharm Sin B* 2022;**12**:1707−22.
13. He X, Wang X, Yang L, Yang Z, Yu W, Wang Y, et al. Intelligent lesion blood−brain barrier targeting nano-missiles for Alzheimer's disease treatment by anti-neuroinflammation and neuroprotection. *Acta Pharm Sin B* 2022;**12**:1987−99.
14. Gopinath A, Collins A, Khoshbouei H, Streit WJ. Microglia and other myeloid cells in central nervous system health and disease. *J Pharmacol Exp Ther* 2020;**375**:154−60.
15. Ising C, Venegas C, Zhang S, Scheiblich H, Schmidt SV, Vieira-Saecker A, et al. NLRP3 inflammasome activation drives tau pathology. *Nature* 2019;**575**:669−73.
16. Gong T, Yang Y, Jin T, Jiang W, Zhou R. Orchestration of NLRP3 inflammasome activation by ion fluxes. *Trends Immunol* 2018;**39**:393−406.
17. Xu X, Xu X, Hao Y, Zhu X, Lu J, Ouyang X, et al. Antispasmodic drug drofenine as an inhibitor of Kv2.1 channel ameliorates peripheral neuropathy in diabetic mice. *iScience* 2020;**23**:101617.
18. Wei Y, Shin MR, Sesti F. Oxidation of KCNB1 channels in the human brain and in mouse model of Alzheimer's disease. *Cell Death Dis* 2018;**9**:820.
19. Frazzini V, Guarnieri S, Bomba M, Navarra R, Morabito C, Mariggio MA, et al. Altered Kv2.1 functioning promotes increased excitability in hippocampal neurons of an Alzheimer's disease mouse model. *Cel Death Dis* 2016;**7**:e2100.
20. Leng L, Yuan Z, Pan R, Su X, Wang H, Xue J, et al. Microglial hexokinase 2 deficiency increases ATP generation through lipid metabolism leading to β-amyloid clearance. *Nat Metab* 2022;**4**:1287−305.
21. Rauchmann BS, Brendel M, Franzmeier N, Trappmann L, Zaganjori M, Ersoezlue E, et al. Microglial activation and connectivity in Alzheimer disease and aging. *Ann Neurol* 2022;**92**:768−81.
22. Lu J, Zhang C, Lv J, Zhu X, Jiang X, Lu W, et al. Antiallergic drug desloratadine as a selective antagonist of 5HT2A receptor ameliorates pathology of Alzheimer's disease model mice by improving microglial dysfunction. *Aging Cell* 2020:e13286.
23. Zhou TT, Quan LL, Chen LP, Du T, Sun KX, Zhang JC, et al. SP6616 as a new Kv2.1 channel inhibitor efficiently promotes β-cell survival involving both PKC/Erk1/2 and CaM/PI3K/Akt signaling pathways. *Cel Death Dis* 2016;**7**:e2216.
24. Jiang B, Aliyan A, Cook NP, Augustine A, Bhak G, Maldonado R, et al. Monitoring the formation of amyloid oligomers using photoluminescence anisotropy. *J Am Chem Soc* 2019;**141**:15605−10.
25. Steiner K, Humpel C. Effects of ischemia on the migratory capacity of microglia along collagen microcontact prints on organotypic mouse cortex brain slices. *Front Cel Neurosci* 2022;**16**:858802.
26. Zhu DY, Lu J, Xu R, Yang JZ, Meng XR, Ou-Yang XN, et al. FX5, a non-steroidal glucocorticoid receptor antagonist, ameliorates diabetic cognitive impairment in mice. *Acta Pharmacol Sin* 2022;**43**:2495−510.
27. Narayanan M, Huynh JL, Wang K, Yang X, Yoo S, McElwee J, et al. Common dysregulation network in the human prefrontal cortex underlies two neurodegenerative diseases. *Mol Syst Biol* 2014;**10**:743.
28. Post MA, Kirsch GE, Brown AM. Kv2.1 and electrically silent Kv6.1 potassium channel subunits combine and express a novel current. *FEBS Lett* 1996;**399**:177−82.
29. Zhang Z, Shen Q, Wu X, Zhang D, Xing D. Activation of PKA/SIRT1 signaling pathway by photobiomodulation therapy reduces Aβ levels in Alzheimer's disease models. *Aging Cell* 2020;**19**:e13054.
30. Zhong L, Xu Y, Zhuo R, Wang T, Wang K, Huang R, et al. Soluble TREM2 ameliorates pathological phenotypes by modulating microglial functions in an Alzheimer's disease model. *Nat Commun* 2019;**10**:1365.
31. Walsh DM, Selkoe DJ. A beta oligomers—a decade of discovery. *J Neurochem* 2007;**101**:1172−84.
32. Lin R, Rao S, Li Y, Zhang L, Xu L, He Y, et al. Conjugation of tacrine with genipin derivative not only enhances effects on AChE but also leads to autophagy against Alzheimer's disease. *Eur J Med Chem* 2021;**211**:113067.
33. Song N, Liu ZS, Xue W, Bai ZF, Wang QY, Dai J, et al. NLRP3 phosphorylation is an essential priming event for inflammasome activation. *Mol Cel* 2017;**68**:185−97. e6.
34. Mulholland PJ, Carpenter-Hyland EP, Hearing MC, Becker HC, Woodward JJ, Chandler LJ. Glutamate transporters regulate extrasynaptic NMDA receptor modulation of Kv2.1 potassium channels. *J Neurosci* 2008;**28**:8801−9.
35. Zeng Z, Xu J, Zheng W. Artemisinin protects PC12 cells against β-amyloid-induced apoptosis through activation of the ERK1/2 signaling pathway. *Redox Biol* 2017;**12**:625−33.
36. Guo X, Lv J, Lu J, Fan L, Huang X, Hu L, et al. Protopanaxadiol derivative DDPU improves behavior and cognitive deficit in AD mice involving regulation of both ER stress and autophagy. *Neuropharmacology* 2018;**130**:77−91.
37. Mielke MM, Aggarwal NT, Vila-Castelar C, Agarwal P, Arenaza-Urquijo EM, Brett B, et al. Consideration of sex and gender in Alzheimer's disease and related disorders from a global perspective. *Alzheimers Dement* 2022;**18**:2707−24.
38. Fisher DW, Bennett DA, Dong H. Sexual dimorphism in predisposition to Alzheimer's disease. *Neurobiol Aging* 2018;**70**:308−24.
39. Bhattacharya S, Haertel C, Maelicke A, Montag D. Galantamine slows down plaque formation and behavioral decline in the 5×FAD mouse model of Alzheimer's disease. *PLoS One* 2014;**9**:e89454.
40. Pluvinage JV, Haney MS, Smith BAH, Sun J, Iram T, Bonanno L, et al. CD22 blockade restores homeostatic microglial phagocytosis in aging brains. *Nature* 2019;**568**:187−92.
41. Sharif H, Wang L, Wang WL, Magupalli VG, Andreeva L, Qiao Q, et al. Structural mechanism for NEK7-licensed activation of NLRP3 inflammasome. *Nature* 2019;**570**:338−43.

42. Subramaniam S, Zirrgiebel U, von Bohlen Und Halbach O, Strelau J, Laliberte C, Kaplan DR, et al. ERK activation promotes neuronal degeneration predominantly through plasma membrane damage and independently of caspase-3. *J Cel Biol* 2004;**165**:357−69.
43. Zhu X, Chen Y, Xu X, Xu X, Lu Y, Huang X, et al. SP6616 as a Kv2.1 inhibitor efficiently ameliorates peripheral neuropathy in diabetic mice. *EBioMedicine* 2020;**61**:103061.
44. Jia Y, Cui R, Wang C, Feng Y, Li Z, Tong Y, et al. Metformin protects against intestinal ischemia−reperfusion injury and cell pyroptosis *via* TXNIP−NLRP3−GSDMD pathway. *Redox Biol* 2020;**32**:101534.
45. Bussian TJ, Aziz A, Meyer CF, Swenson BL, van Deursen JM, Baker DJ. Clearance of senescent glial cells prevents tau-dependent pathology and cognitive decline. *Nature* 2018;**562**:578−82.
46. Rice HC, de Malmazet D, Schreurs A, Frere S, Van Molle I, Volkov AN, et al. Secreted amyloid-β precursor protein functions as a $GABA_BR1a$ ligand to modulate synaptic transmission. *Science* 2019; **363**:eaao4827.
47. Suh J, Romano DM, Nitschke L, Herrick SP, DiMarzio BA, Dzhala V, et al. Loss of Ataxin-1 potentiates Alzheimer's pathogenesis by elevating cerebral BACE1 transcription. *Cell* 2019;**178**: 1159−75.e17.
48. Ulland TK, Song WM, Huang SC, Ulrich JD, Sergushichev A, Beatty WL, et al. TREM2 maintains microglial metabolic fitness in Alzheimer's disease. *Cell* 2017;**170**:649−63.e13.
49. Huang YA, Zhou B, Wernig M, Sudhof TC. ApoE2, ApoE3, and ApoE4 differentially stimulate APP transcription and Aβ secretion. *Cell* 2017;**168**:427−41. e21.
50. Ennerfelt H, Frost EL, Shapiro DA, Holliday C, Zengeler KE, Voithofer G, et al. SYK coordinates neuroprotective microglial responses in neurodegenerative disease. *Cell* 2022;**185**:4135−52. e22.
51. Yoo JM, Lee BD, Sok DE, Ma JY, Kim MR. Neuroprotective action of *N*-acetyl serotonin in oxidative stress-induced apoptosis through the activation of both TrkB/CREB/BDNF pathway and Akt/Nrf2/Antioxidant enzyme in neuronal cells. *Redox Biol* 2017;**11**: 592−9.
52. Shi Y, Manis M, Long J, Wang K, Sullivan PM, Remolina Serrano J, et al. Microglia drive APOE-dependent neurodegeneration in a tauopathy mouse model. *J Exp Med* 2019;**216**:2546−61.
53. Arechiga-Figueroa IA, Delgado-Ramirez M, Moran-Zendejas R, Rodriguez-Menchaca AA. Modulation of Kv2.1 channels inactivation by curcumin. *Pharmacol Rep* 2015;**67**:1273−9.
54. Yeh CY, Ye ZF, Moutal A, Gaur S, Henton AM, Kouvaros S, et al. Defining the Kv2.1-syntaxin molecular interaction identifies a first-in-class small molecule neuroprotectant. *Proc Nat Acad Sci U S A* 2019; **116**:15696−705.
55. Bodur E, Cokugras AN, Tezcan EF. Inhibition effects of benactyzine and drofenine on human serum butyrylcholinesterase. *Arch Biochem Biophys* 2001;**386**:25−9.